Annual 30-meter Dataset for Glacial Lakes in High Mountain Asia from 2008 to 2017

Fang Chen[1,2,3], Meimei Zhang[1], Huadong Guo[1,2,3], Simon Allen[4,5], Jeffrey S. Kargel[6], Umesh K. Haritashya[7], C. Scott Watson[8]

[1]Key Laboratory of Digital Earth Science, Aerospace Information Research Institute, Chinese Academy of Sciences, No. 9 Dengzhuang South Road, Beijing 100094, China.

[2]State Key Laboratory of Remote Sensing Science, Aerospace Information Research Institute, Chinese Academy of Sciences, No. 9 Dengzhuang South Road, Beijing 100094, China.

[3]Hainan Key Laboratory of Earth Observation, Aerospace Information Research Institute, Chinese Academy of Sciences, Sanya 572029, China.

[4]Department of Geography, University of Zurich, Zurich, 8057, Switzerland.

[5]Institute for Environmental Sciences, University of Geneva, Geneva 1205, Switzerland.

[6]The Planetary Science Institute, Tucson, Arizona, 85719, USA.

[7]Department of Geology, University of Dayton, Dayton, Ohio, 45469, USA.

[8] Department of Hydrology & Atmospheric Sciences, University of Arizona, Tucson, Arizona, 85721, USA.

Correspondence to: Meimei Zhang (zhangmm@radi.ac.cn)

Abstract. Atmospheric warming is intensifying glacier melting and lake development in High Mountain Asia (HMA), which could increase glacial lake outburst flood hazards and impact water resource and hydroelectric power management. There is a pressing need for obtaining the comprehensive knowledge of the distribution, area of glacial lakes, and also quantification of variability in their size and type at high resolution in HMA. Here, we developed a HMA Glacial Lake Inventory (Hi-MAG) database to characterize the annual coverage of glacial lakes from 2008 to 2017 at 30 m resolution using Landsat satellite imagery. It can be observed that glacial lakes exhibited total area increases of 90.14 km^2 between 2008-2017, a +6.90% change relative to 2008 (1305.59 ± 213.99 km^2). Annual increase in lake number and area are 306 glacial lakes and 12 km^2, respectively, and maximum increased lake number occurred in 5400 m elevation, which increased by 249. Proglacial lake dominated areas such as the Nyainqentanglha and Central Himalaya, where around more than half of the glacial lake area (summed over 1°×1° grid) consisted of proglacial lakes showed obvious lake area expansion, while in the regions of Eastern Tibetan Mountains and Hengduan Shan, the unconnected glacial lakes occupied about over half of the total lake area in each grid, exhibited stability or slight reduction. Our results demonstrate proglacial lakes are a main contributor to recent lake evolution in HMA, accounting for 62.87% (56.67 km^2) of the total area increase. Proglacial lakes in the Himalaya ranges alone accounted for 36.27% (32.70 km^2) of the total area increase. Regional geographic variability of debris cover, together with trends in warming and precipitation over the past few decades, largely explain the current distribution of supra- and proglacial lake area across HMA. The Hi-MAG database is available at: https://doi.org/10.5281/zenodo.4059181 (Chen et al., 2020), it can be used for studies on the complex interactions between glacier, climate and glacial lake, glacial lake outburst floods, potential downstream risks and water resources.

1 Introduction

High Mountain Asia (HMA) consisting of the whole Tibetan Plateau and adjacent mountain ranges such as Himalaya, Karakoram, and Pamirs, covers the largest area of mountainous glaciers globally. Atmospheric warming has resulted in widespread glacier retreat and downwasting in many mountain ranges of the HMA (Brun et al., 2017b;Bolch et al., 2012b), which favor the formation and development of a large amount of glacial lakes, yet glacial lakes have been incompletely documented at small time intervals. Glacial lake development varies according to climatic, cryospheric, and lake-specific conditions, such as basin geometry that is either connected to glaciers or unconnected, and the length of the lake/glacier contact (Zhao et al., 2018).

Many previously published researches have devoted to the glacial lakes mapping with remotely sensed data over the different regions of HMA. Some works mainly focus on the investigation of the development of relatively large glacial lakes. Rounce et al. identified 131 glacial lakes in Nepal in 2015 that are greater than 0.1 km^2 (Rounce et al., 2017). Li et al. compiled an inventory of glacial lakes (⩾0.01 km^2) with a spatial resolution of 30 m in the Karakoram mountains (Li et al., 2020). Aggarwal et al. shared a new dataset of glacial and high-altitude lakes that have an area > 0.01 km^2 for Sikkim, Eastern Himalaya from 1972–2015 (Aggarwal et al., 2017). Ukita et al. constructed a glacial lake inventory of Bhutan in the Himalaya from the period 2006-2010 based on high-resolution PRISM and AVNIR-2 data from ALOS. Considering small lakes present less of a GLOF risk. They set 0.01 km^2 as the minimum lake size (Ukita et al., 2011). Ashraf et al. used Landsat-7 ETM+ images for the 2000-2001 period to delineate glacial lakes greater than 0.02 km^2 in the Hindukush-Karakoram-Himalaya (HKH) Region of Pakistan (Ashraf et al., 2012). Because small glacial lakes experience highly variable in their shape, location, and occurrence, and were clearly sensitive to the warming climate and glacier wastage, a growing number of scholars have paied attention to the abundance of small glacial lakes. Salerno et al. provided a complete mapping of glacial lakes (including lake size less than 0.001 km^2) and debris-covered glaciers with 10-m spatial resolution in the Mount Everest region in 2008 (Salerno et al., 2012). Wang et al. utilized Landsat TM/ETM+ images for the years 1990, 2000 and 2010 to map glacial lakes with area more than 0.002 km^2 in Tien Shan Mountains (Wang et al., 2013a). Luo et al. examined glacial lake changes (lake area >0.0036 km^2) for the entire western Nyainqentanglha range for the five periods between 1976 and 2018 using multi-temporal Landsat images (Luo et al., 2020). International Centre for Integrated Mountain Development (ICIMOD) provided comprehensive information about the glacial lakes (greater than or equal to 0.003 km^2) of five major river basins of the Hindu Kush Himalaya (HKH) using Landsat images for the year 2005 (Sudan et al., 2018). Nie et al. mapped the distribution of glacial lakes across the entire Himalaya in the year of 2015 using a total of 348 Landsat images at 30 m resolution. They set the minimum mapping unit to 0.0081 km^2 (Nie et al., 2017). Zhang et al. presented a database of glacial lakes larger than 0.003 km^2 in the Third Pole for the years ~1990, 2000, and 2010 (Zhang et al., 2015). All these researches greatly help to fill the data gap of glacial lakes information in the HMA region. At the global scale, Pekel et al. used millions of Landsat satellite images to record global surface water over the past 32 years at 30-metre resolution (Pekel et al., 2016b), many large and visible glacial lakes were also included. More recently, Shugar et al. mapped glacial lakes with areas >0.05 km^2 around the world using 254,795 satellite images from 1990 to 2018 (Shugar et al., 2020). Wang et al. developed a glacial lake inventory (with size of larger than 0.0054 km^2) across the High Mountain Asia at two time periods (1990 and 2018) using manual mapping on 30 m Landsat images (Wang et al., 2020b). They firstly introduce glacial lake inventory at such a large-scale, the data shared will be served as a baseline for the further studies related to water resource assessment or glacier hazard risk.

In summary, a homogeneous, annually resolved inventory and analysis of the spatial and temporal extent of different types of glacial lakes over the entire HMA has still been lacking. We developed a HMA Glacial Lake Inventory (Hi-MAG) database to characterize the annual coverage of glacial lakes from 2008 to 2017 at 30 m resolution. 40,481 Landsat scenes were processed using Google Earth Engine (GEE) cloud computing to delineate glacial lakes (located within 10 km from the nearest glacier terminus) larger than nine (e.g., 3 x 3) pixels (0.0081 km^2) (Nie et al., 2017).

Lakes were manually classified into four categories according to their position relative to the parent glacier or their formation mechanisms (Fig. A1): i) proglacial lakes, usually connected to the glacier tongue and dammed by glacier ice, unconsolidated or ice-cemented moraines (mixture of ice, snow, rock, debris and clay, etc.), proglacial lakes are located next to the glacier terminus and receive melt water directly from their mother glaciers; ii) supraglacial lakes - this is where ponds form in depressions on low-sloping parts of the surface of a melting glacier and are dammed by ice or the end-moraine or stagnating glacier snout; iii) unconnected glacial lakes, which are glacial lakes not directly connected to their parent glaciers at the present time but which, to some extent, may be fed by at least one of the glaciers located in the basin and may have been (but not necessarily are) recently detached from ice contact due to glacial recession. Although not directly connected with the parent glaciers, these glacial lakes are also the outcome of glacier melting in response to atmospheric warming, they can supply fresh water to major river systems of the HMA region, and their changes have significant scientific and socio-economic implications (Nie et al., 2017;Song et al., 2016); and (iv) ice-marginal lakes, these lakes are generally distributed on one side of the glacier tongue, which means that the lake is dammed by the glacier ice on this side. While on the other side, it is bounded by a lateral moraine. With the increase of atmospheric warming and accelerated melting of glacier, some glacier tributary gradually detaches from a main trunk glacier. The detached location, where glacier melting has been particularly intense, in some case is also likely to form ice-marginal lakes. We note that such ice-marginal lakes are very common in some parts of the world (e.g., Alaska) (Armstrong and Anderson, 2020;Capps et al., 2011) but are not common in HMA. Besides, purely glacier-dammed lakes are formed by the advance of glaciers and dammed by almost pure glacier ice. Although the dam composition and structure is slightly different between the proglacial lakes and glacier-dammed lakes, because they are all located in the front of the glacier tongue and driven by the mother glacier, in the process of appending attributed information to each glacial lake, glacier-dammed lakes were merged into class of proglacial lakes.

Every lake was cross-checked manually for its boundary and attribution. We defined an uncertainty of 1 pixel for the detected glacial lake boundaries, and calculated the lake area error for the whole HMA region. We also assessed the inventory for climatic and geomorphological influences on lake distribution across HMA.

2 Study area and data

2.1 Study area

The term HMA refers to a broad high-altitude region in South and Central Asia that covers the whole Tibetan Plateau and adjacent mountain ranges, including the Eastern Hindu Kush, Western Himalaya, Eastern Himalaya, Central Himalaya, Karakoram, Western Pamir, Pamir Alay, Northern/Western Tien Shan, Dzhungarsky Alatau, Western Kunlun Shan, Nyainqentanglha, Gangdise Mountains, Hengduan Shan, Tibetan Interior Mountains, Tanggula Shan, Eastern Tibetan Mountains, Qilian Shan, Eastern Kunlun Shan, Altun Shan, Eastern Tien Shan, Central Tien Shan, Eastern Pamir (Fig. 1 and Fig. 6a). It extends from 26°N to 45°N and from 67°E to 105°E, the altitude of the plateau is about 4500 m on average (Baumann et al., 2009). It's made up of alternating mountains, valleys and rivers, the terrain is fragmented, showing a decreasing terrain from Northwest to Southeast. HMA has a series of East-West mountains that occupy most of the area. Among these, Tanggula Shan lies in the central part of the HMA, with an altitude of over 6000 m. The height of fifteen highest mountains in the Himalayas are more than 8000 m, while the peaks of the mountains in the northern plateau are more than 6500 m. The North-South mountains are mainly distributed in the southeast of the plateau and near the Hengduan Mountain area. These two groups of mountains constitute the geomorphic framework and control the basic pattern of the plateau landform. Continuous and discontinuous permafrost have developed on the higher land and north facing slopes.

HMA is the source of several of Asia's major rivers, including the Yellow, Yangtze, Indus, Ganges, Brahmaputra, Irrawaddy, Salween, and Mekong. They play a crucial role in downstream hydrology and water availability in Asia (Immerzeel and Bierkens, 2010). Most glaciers in the Tibetan Plateau are retreating, except for the Western Kunlun (Neckel et al., 2014;Kääb et al., 2015) and the Karakoram, where a slight mass gain is occurring (Bolch et al., 2012a;Gardner et al., 2013). Moreover, glaciers in different mountain ranges show contrasting patterns. Local factors (e.g., exposure, topography, and debris coverage) may partly account for these differences but the spatial and temporal heterogeneity of both the climate and degree of climate change may be the main reason. Glacial lakes are formed and developed temporally with the retreat or thinning of glaciers and are directly or indirectly fed by glacier meltwater, they are located within 10 km from the nearest glacier terminus (Zhang et al., 2015;Wang et al., 2013b).

The HMA climate is under the combined and competitive influences of the East Asian and South Asian monsoons and of the westerlies (Schiemann et al., 2009). This unique geographical position produces an azonal plateau climate characterized by strong solar radiation, low air temperatures, large daily temperature variations and small differences between annual mean temperatures (Yao et al., 2012). The annual mean temperature is 1.6 °C, with the lowest temperature of −1 – −7 °C occurring in January and the highest temperature of 7 – 15°C occurring in July. The cumulative precipitation is about 413.6 mm a year.

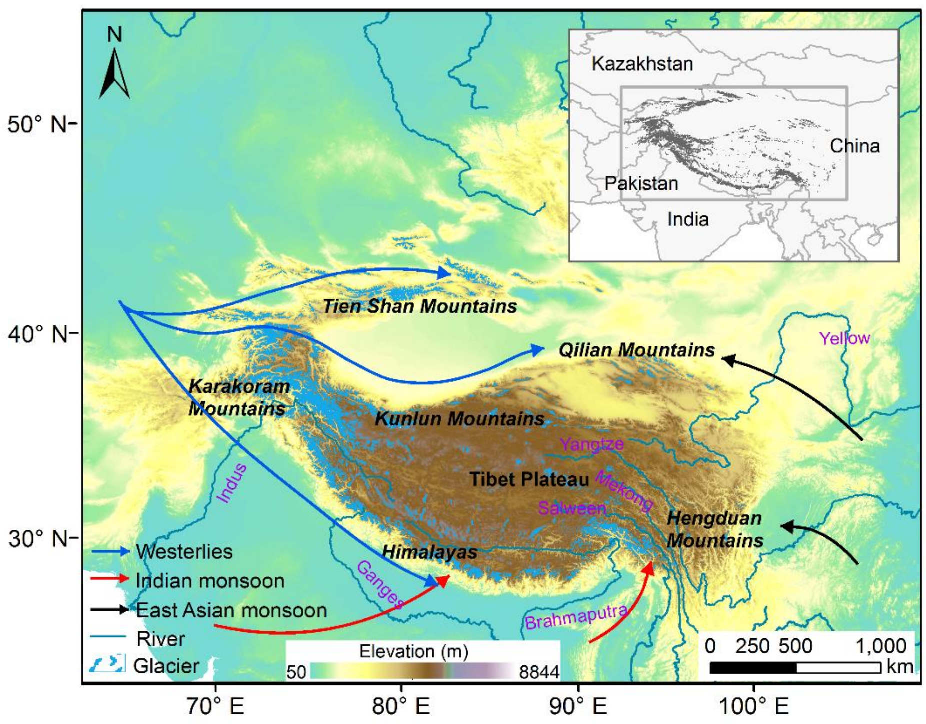

Fig. 1. The location of the High Mountain region of Asia (HMA). Glacier outlines from the Randolph Glacier Inventory (RGI v5.0), the Second Chinese Glacier Inventory (CGI2) and the GAMDAM inventory are drawn in sky blue.

2.2 Dataset

40,481 satellite images including Landsat 5 TM imagery during 2008 to 2011, Landsat 7 ETM+ imagery in 2012, and Landsat 8 OLI during 2013 to 2017, were available in GEE and were used to produce the annual glacial lake maps over the entire HMA (Fig. 2). Here, when Landsat 5 or 8 data were available, Landsat 7 ETM+ imagery with SLC-off gaps were generally excluded due to their artefacts induced by the slatted appearance of the original images, but were exclusively used for the glacial lake mapping in 2012 since no other Landsat data were acquired that year. For the years before 2008, all the available Landsat 5 TM data in each year (e.g., 2004, 2005, 2006, and 2007) do not fully cover the HMA region.

The SLC-off condition of Landsat ETM+ introduces artefacts because the slatted appearance of the original images is occasionally carried into the glacial lake map in 2012. Techniques to fill the SLC-off gaps exist, but these create artificial values that will result in false detections of water (Chen et al., 2011). Considering the strong spatial and temporal variability of glacial lakes like supraglacial lakes, techniques which merge data from one or more SLC-off fill scenes for generation of a gap-free image require careful use, even using the thousands of Landsat ETM+ images. It is noted water mapping using multi-temporal time series images at large scales usually avoided the use of such techniques (Mueller et al., 2016). Therefore, Landsat 7 ETM+ data with intensive slatted appearance is not really a good and suitable data for the classification of numerous of glacial lakes. In this study, because the only useable data source for the year of 2012 is from Landsat 7 ETM+, to ensure continuity of annual data from 2008 to 2017, we have tried our best to manually extract the glacial lakes from the 2012 ETM+ images as accurately as possible.

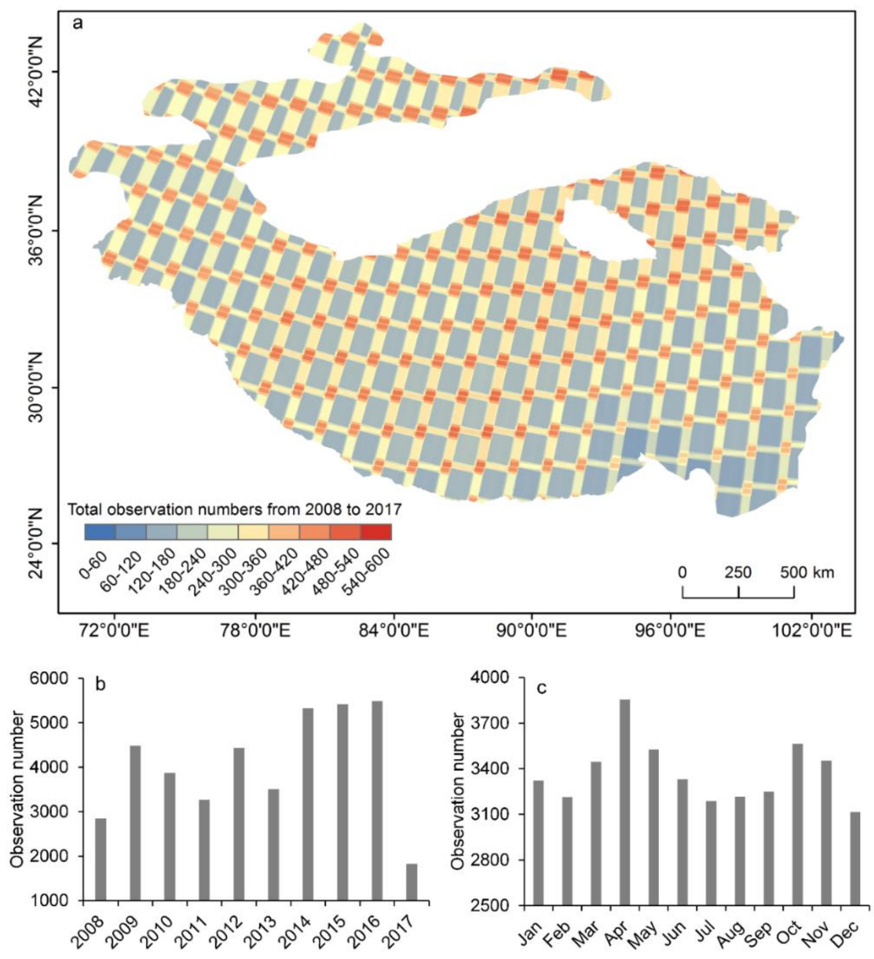

Fig. 2. (a) The distribution of total observation numbers from all GEE Landsat scenes by (b) year and (c) month.

3 Methods

3.1 Satellite imagery selection strategy

To reduce the influence of seasonal lake fluctuations for the mapping, one effective solution is to map glacial lakes and measure their long-term changes during stable seasons when lake extents are minimally affected by meteorological conditions and glacier runoff. Here the selected time series of Landsat data were generally from July to November based on the analyses of mapping time of glacial lakes in the different regions. During this period of each year, the Landsat imagery featured less perennial snow coverage. Change in area of glacial lake is minor and has a large area following the glacier runoff and precipitation (Zhang et al., 2015;Nie et al., 2017;Chen et al., 2017). The lakes may also reached their maximum extent around the end of the glacier ablation season (June to August) (Gardelle et al., 2013;Liu et al., 2014)- except in the central and eastern Himalaya, where peak ablation extends into post-monsoon September and October. In monsoon-affected areas such as Nepal and Bhutan, monsoon cloud cover in July to mid-September means that most of those areas are covered by clear-sky images only from late September to November. Southeast Tibet regions are problematic not only because the observation season is short but abundant cloud cover, which is formed by the warm humid airflow raised by topography (Haritashya et al., 2018;Qiao et al., 2016;Zhang et al., 2020). As the most highly variable glacial lakes in the study area, supraglacial lakes change preferentially in the year, showing an increase in area during the pre-monsoon, and rising to the peak area in the early monsoon (June to July) (Miles et al., 2017a;Miles et al., 2017b). Although the selected image seasons are slightly different due to the meteorological conditions in different regions, they all comply with the same criterion that lake area were in clear-sky images and has small snow coverage. This will ensure the initial reliability of the mapping glacial lakes through GEE cloud computing platform. If no valid observations can be obtained, then optimal mapping time needs to be broaden during the whole year.

To further increase data availability, and also as the basis for data selection in the periods beyond the optimum mapping time, we set two criteria for the selection of imagery with valid observations over the potential glacial lake area by using the cloud score functions in GEE, including (i) cloud cover is less than 20% in the 10 km buffer around each glacier outlines of a Landsat scene, or (ii) less than 20% cloud cover for the entire scene. The cloud score functions in GEE may face a big challenge to detect clouds in mountain headwaters with high snow and ice cover, large amounts of snow and ice are likely to be identified as clouds. However, in this study, it is a much stricter criteria to filter out more images with lots of cloud or cloud-lookalike objects (snow/ice) and finally choose images with good observations.

3.2 Extraction of glacial lake outlines

For the development of HMA Glacial Lake Inventory (Hi-MAG) database, we applied a systematic glacial lake detection method that combined two steps from initial glacial lake extraction and subsequently manual refinement of lake mapping results. The main procedures for glacial lake mapping using Landsat data are (Fig. 3): (i) the Landsat top of atmosphere data were clipped according to the extent of the glacier buffers and assembled into a time-series dataset; (ii) poor quality observations were identified - these included areas affected by cloud, cloud shadow, topographic shadow and SLC-off gaps. Here we used the Fmask routine (Zhu and Woodcock, 2012) to detect the clouds and cloud shadows in an imagery. Fmask has the advantage of being able to process a large number of images in a computationally efficient way. Topographic shadows are located in the areas where the sunlight is blocked, generally on the dark side of the high mountains, their surface gradients are great and the terrain reliefs are small. Therefore, topographic shadows were masked using the slopes (larger than 10°) and shaded relief values (less than 0.25) calculated from SRTM data (Li and Sheng, 2012;Quincey et al., 2007). This will remove considerable mountain shadows that have the similar spectral reflectance with water bodies. However, SRTM DEM was generated in 2000, which is different from the acquisition time of Landsat images used for the glacial lake mapping in this study, the derived slopes and shaded relief cannot fully represent the conditions on the date a given Landsat scene is acquired. As a consequence, some lakes that have grown at steep glacier tongue may be masked, and some mountain shadows that interfere with the mapping results of glacial lakes from GEE still remain, leading to the fact that glacial lakes in the steep areas are omitted, and residual shadows are misclassified as glacial lakes. As for the SLC-off gaps in the ETM+ images, lakes out of the gaps were accurately classified, but if glacial lakes are covered by gaps, they will be misclassified. Errors caused by striped gaps of Landsat ETM+ were manually corrected using additional high-quality scenes during the whole year with assistance of images from adjacent years. (iii) the modified Normalized Difference Water Index (MNDWI) was calculated (Hanqiu, 2006); (iv) the potential glacial lake areas were extracted by applying adaptive MNDWI threshold (Li and Sheng, 2012). To define a glacial lake in the image, the minimum number of water pixels was inconsistent in different studies. For example, Zhang et al., 2015 set the smallest detectable glacial lakes in the Third Pole of larger than 0.0027 km^2 (three connected pixels) using the Landsat TM/ETM+ data. Nie et al., 2017 selected 0.0081 km^2 (nine connected pixels) as the minimum mapping unit to map glacial lakes in the Himalaya. Other studies set the minimum threshold areas as 0.001km^2 (Salerno et al., 2012), 0.002km^2 (Wang et al., 2013a), 0.0036km^2 (Luo et al., 2020), 0.0054km^2 (Wang et al., 2020b), 0.01km^2 (Li et al., 2020) for the identification of glacial lakes and analysis of their spatial and temporal variations. A smaller minimum mapping unit will detect more glacial lakes, however, the uncertainty it brings is also larger than large lakes at the same resolution (Salerno et al., 2012). Our results demonstrate that a lake area covering fewer than nine water pixels have an area error of larger than 50% (Please see the Section 4). Given the area uncertainty of glacial lakes and the spatial resolution of Landsat data, in this study, glacial lakes larger than nine pixels ($\geq$ 0.0081 km^2) were considered as the minimum mapping unit; and (v) manual inspection and refinement of individual glacial lake were conducted and the related attribution were added for each lake.

Based on the automated processing, nearly 60% glacial lakes in each year can be correctly classified, of the other lakes that were not properly classified, 30% were missed and 10% were misclassified. For such a large-scale area that characterized by various and complex climatic, geological and terrain conditions, this classification method is simple but effective, the results are also reasonable since it provides very low commission errors. To ensure the quality of inventory, strict quality control was conducted to visually inspect and correct the mapping errors after the automated processing using GEE. False lake features, mainly identified as mountain shadows and river segments, were manually removed by overlapping mapped lake shorelines on the source Landsat imagery and higher-resolution imagery in Google Earth. For missing glacial lakes, such as some lakes may be covered by ice and clouds for years, grow at steep glacier tongues, and lakes show heterogeneous reflectance with the surrounding backgrounds, the lake boundaries were edited further using ArcGIS. Furthermore, a cross-check and modification was conducted for each glacial lake based on the lake mapping results in conjunction with multi-temporal Landsat imagery. Here all the Landsat imagery that used for the inspection were downloaded manually from USGS Earth Explorer website (https://earthexplorer.usgs.gov/). Outputs per lake polygon include the information about lake type, elevation, Euclidian distance to the nearest glacier terminus, area and perimeter. Noted that if there are more than one suitable satellite images in a year, image with the least cloud cover will be selected for the calculation of the area and perimeter of a given lake. Meanwhile, each mountain range was characterized individually by utilizing the mountain boundary shapefile in High Mountain Asia (geo.uzh.ch/~tbolch/data/regions_hma_v03.zip).

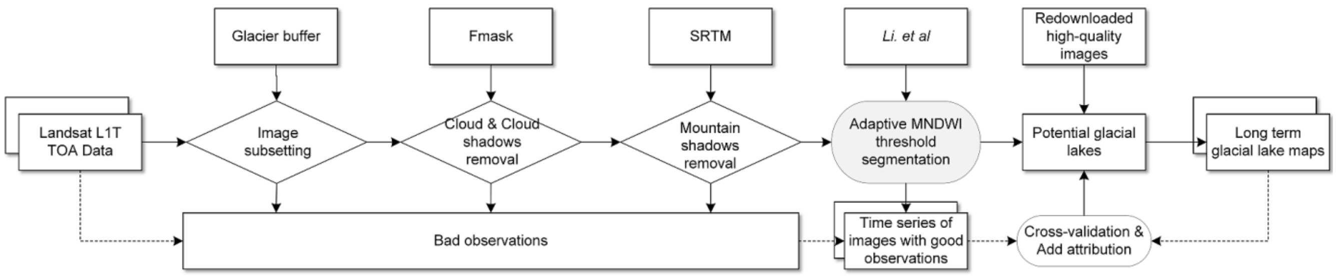

Fig. 3. Diagram of the glacial lake mapping workflow.

3.3 Yearly lake area changes calculations

Based on the final generated lake inventory data, we used the slope of linear regression of lake area (over the grid cell of 1°×1°) versus mapping year to qualify the yearly lake area changes during the study period. The approach to change analysis was predicted using a Theil-Sen estimator, which chooses the median slope among all the derived fitted lines, can effectively represent long-term area changes due to its robustness for the trend detection and insensitivity to outliers, it is also useful for the elimination of the effect from differences in the sensor performance for the mapping of glacial lakes (Kumar, 1968;Song et al., 2018). Although all the lake were manually checked and edited, due to the limitation of available images and other factors, the conditions of glacial lake mapping are not perfectly consistent for each year. For example, the image dates are not consistent across the whole HMA region because of atmospheric disturbances, also the influences from varying lake characteristics, image quality (Bhardwaj et al., 2015;Thompson et al., 2012), ice and shadow that obscured the lakes, which all contributed to the detection errors in the lake extent and their annual variation. Generally, these errors are objective and acceptable as a result of the nature of the limited remote sensing data. For this study, because we used long time series (10 years) data for the estimation of annual lake area change, and also the errors only accounts for a small proportion of the total glacial lake area for each year, errors in the observed lake area caused by the different effects do not apparently affect the trend statistical results. For the glacial lake area time series in each 1°×1°grid, we applied the Theil-Sen estimator to smooth the annual time series of data and derive the slope (annual change) of the trend. A Mann-Kendall trend test was used to detect and further confirm the statistical confidence by the linear regression results. All the estimated trends fall within the 90% confidence intervals. The upper and lower change estimates that satisfy the 90% confidence interval for the slope were also derived over the whole HMA region (Fig. A2).

4 Cross-validation and uncertainty estimate

Accuracy assessment of the mapping results is difficult due to the lack of field measurements of glacial lakes in the continental-scale area like HMA. To obtain the quality controlled data, the glacial lake vector over the entire HMA for the years from 2008 to 2017 has been rechecked and reedited individually through dynamic cross-validation by ten trained experts, which is a time consuming process but are essential to maximize the quality of glacial lake change detection.

For the estimation of the uncertainty of glacial lake area, a key influence factor is the spatial resolution of satellite data. In this study, the uncertainty of the glacial lake area was estimated as an error of ±1 pixels on either side of the delineated lake boundary. The percentage error of area determinations, A_{er}, then is proportional to sensor resolution and is given by (Krumwiede et al., 2014):

$$A_{er} = 100 \cdot (n^{1/2} \cdot m) / A_{gl} \tag{1}$$

Where *n* refers to the number of pixels on the boundary of a glacial lake, approximated by the ratio of the perimeter length and spatial resolution, *m* is the area of a pixel in the Landsat image (m^2), A_{gl} is the lake area (m^2) and the factor 100 is there to convert to percentage.

Assuming an uncertainty of 1 pixel for the detected glacial lake boundaries, we calculated the systematic errors for the whole HMA region (Fig. 4). For the year between 2008 and 2017, the area uncertainty of each glacial lake generally ranged from 0.30% to 50%, with the mean value falling around the 17%, and standard deviation around 11% (Fig. 4a). The maximum and mean value of area uncertainty for the glacial lakes in 2010 are the lowest, while for the year of 2016, the corresponding statistics are highest, this can be attributed to the different factors. The maximum of area uncertainty of glacial lakes is related with the shape and size of a certain lake (as can be seen from equation (1)), but its mean value is equal to the sum of the area uncertainties of each glacial lake divided by the total number, which depend on the total number of glacial lakes in a year, and also the shape and area of each lake. Besides, a close relationship can be found between the area uncertainties and the sizes of the glacial lakes (Fig. 4b). Most of the large glacial lakes (area ≥ 0.04km^2) have the mean area uncertainty of about 7%. This systematic errors were more significant for the small-sized glacial lakes. We measured glacial lake down to 0.0081 km^2 (nine pixels in Landsat imagery), where systematic errors calculated by equation (1) were ~50%.

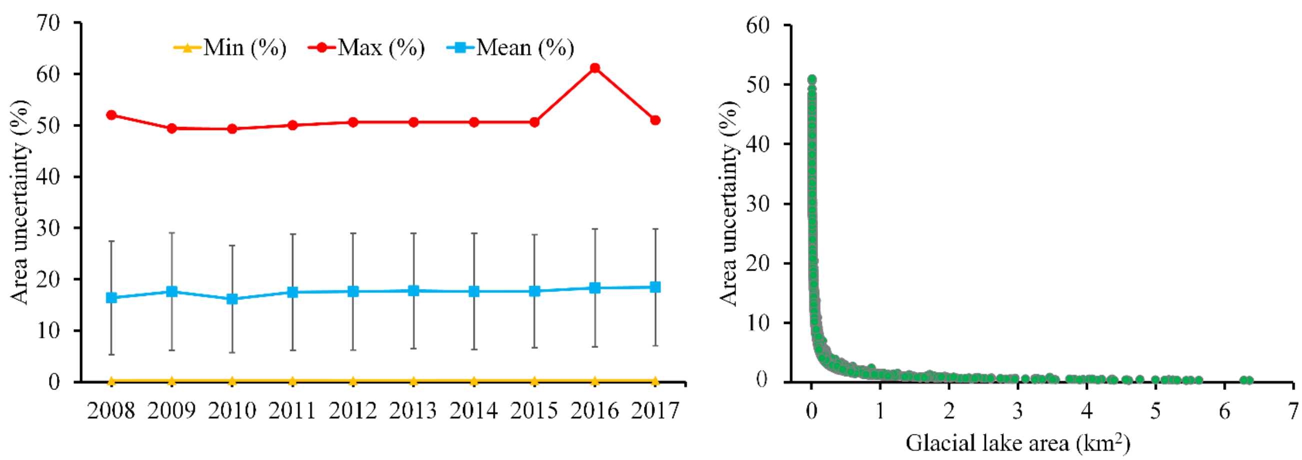

Fig. 4. (a) Statistics of area uncertainty (%) of glacial lakes for the years from 2008 to 2017. (b) Relationship between area uncertainties and areas of all the glacial lakes in HMA in 2017.

5 Results

5.1 Distribution of various types and sizes of glacial lakes

The area coverage of glacial lakes increased by 90.14 km^2 between 2008-2017, a 6.90% increase relative to 2008 (1305.59 ± 213.99 km^2) (Fig. 5a). A Theil-Sen regression fit to all the data showed a mean expansion rate of 12 km^2 a^{-1} for the 10-year record (Fig. 5a). Meanwhile, the estimated changes in glacial lake number from 2008 (12,593 lakes) to 2017 (15,348 lakes) showed an average increase of 306 lakes a^{-1}. The steeper percentage increase in lake number (22.33%) compared to a slower area expansion (8.79%) based on their linear fit trends showed that many small glacial lakes formed over this decade. The number of lakes increased most rapidly above 4400 m a.s.l., especially above 5300 m (Fig. 5b). The increase of proglacial lakes was concentrated above 4900 m (Fig. 5c). Unconnected glacial lakes grew very slightly in total area below 4400 m (Fig. 5d), but increased at higher elevations. Glaciers are retreating and thinning at ever-higher elevations (Nie et al., 2017), causing the formation of new supraglacial lakes at high-elevation, expansion of existing ice-contact lakes, and detachment of glaciers from some lakes.

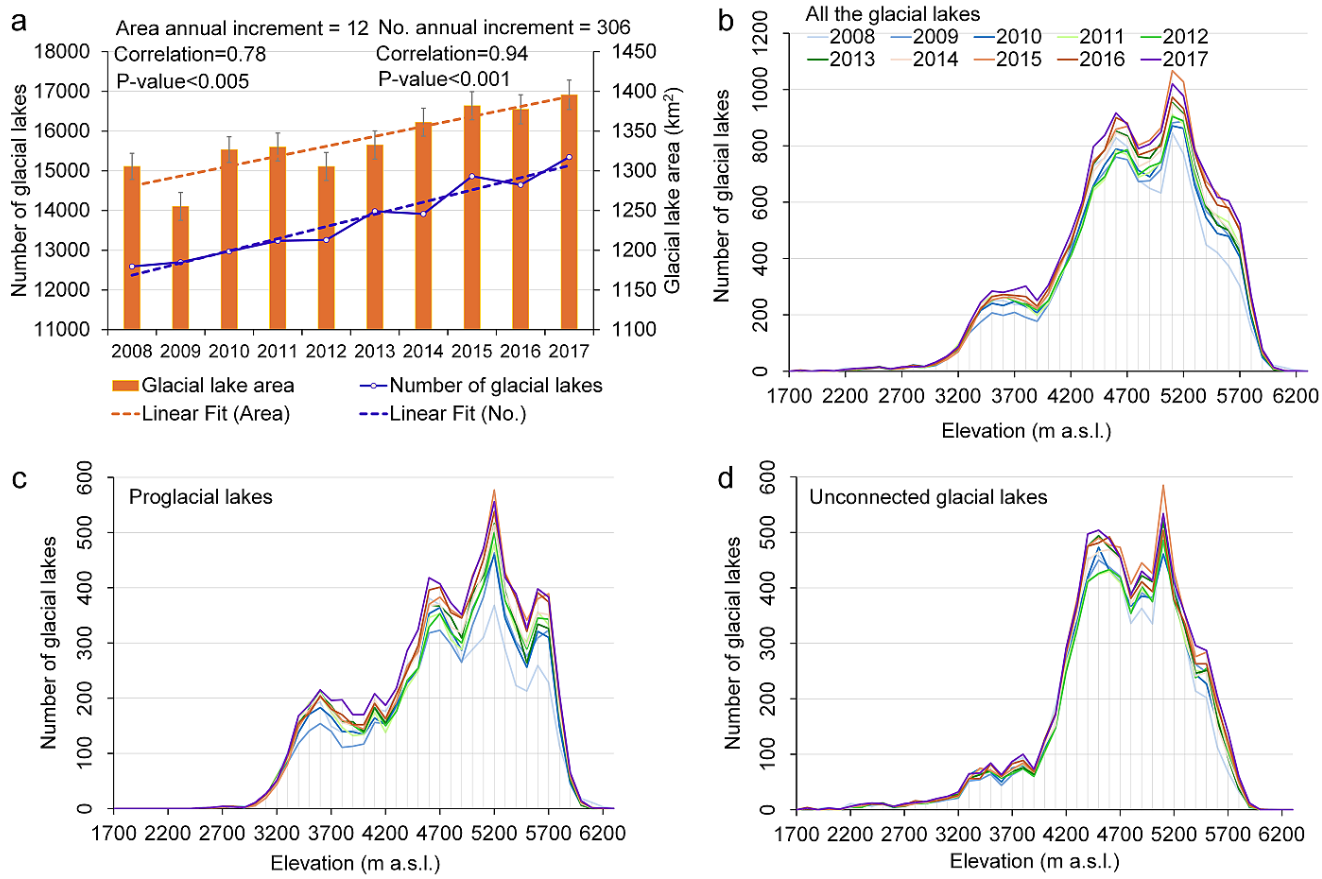

Fig. 5. Annual glacial lake number and area. (a) Total number and area of glacial lakes for HMA between 2008-2017. The annual increment is the slope of the trend of annual lake area and number. Altitudinal distribution (100-m bin sizes) of lake numbers for **(b)** all glacial lakes, **(c)** proglacial lakes, and **(d)** unconnected glacial lakes.

Annual changes in glacial lakes were further analyzed spatially using a 1°×1° grid over 22 mountain regions (Fig. 6a) using Theil-Sen regression analysis. An analysis on mountain-wide lake area loss/gain from 2008 to 2017 was conducted (Table A1). Negative or undiscernible changes in glacial lake area were observed in the Eastern Tien Shan, Eastern Hindu Kush, Hengduan Shan and Eastern Tibetan Mountains (Fig. 6b), thus reducing overall increasing glacial lake area in HMA. The Eastern Hindu Kush lost 2.8 km^2 of lake area (Table A1), with the negative area change (-0.43 $km^2\ a^{-1}$) near 35°N, 73°E. Glacial lakes in Nyainqentanglha, Gangdise Mountains exhibited area loss and gain in some regions. In contrast, Central and Eastern Himalaya, Central Tien Shan showed rapid lake area increases. Between 2008 and 2017 Central Himalaya's glacial lake area increased by 27.09 km^2 (Table A1), exhibiting both a high density of 47 glacial lakes per 100 km^2 in 2017 (Fig. A3) and rapid growth, +0.94 $km^2\ a^{-1}$, in lake area due to retreat and thinning of debris-covered glaciers (Song et al., 2016). Moderate area gains occurred along most of the Western Kunlun and Tanggula Shan, e.g., +0.38 $km^2\ a^{-1}$ in Tanggula Shan. Glacial lake area in Pamir Alay, Eastern Pamir and Eastern Kunlun Shan was spatially and temporally invariant across the whole observation record.

We found that glacial lakes exhibited different expansion trends for different lake types and supraglacial and ice-marginal lakes have relative few coverage areas comparing with proglacial and unconnected lakes (Fig. 6b and Fig. 6c). In the Nyainqentanglha and Central Himalaya, around half of the glacial lake area consisted of proglacial lakes, where most growth occurs. In the negative lake growth (shrinkage) regions of Eastern Tibetan Mountains and Hengduan Shan, the unconnected glacial lakes were dominantly occupied. As the interaction with the glacier gradually weakened, part of the water source supplied by glaciers is reduced. Also, combined with the effects from atmospheric warming and decrease of precipitation, regions mainly consist of unconnected glacial lakes show the decreasing trend in area. Proglacial lakes contributed approximately 62.87% (56.67 km^2) of total area increase over HMA (Table A1 and A2). Proglacial lakes in the Central Himalaya, Eastern Himalaya, and Western Himalaya, accounted for 36.27% (32.70 km^2) of the total area increase. In general, proglacial lakes are a main contributor to recent lake evolution in HMA.

We also noted the large area growth of lakes occurred in areas with relatively large proportion of small glacial lakes, mainly due to rapid growth of existing lakes and new lake formation (Fig. 6d). For example, in some areas of Central and Eastern Himalaya, Nyainqentanglha that have large annual increase in lake area (higher than 0.23 km^2a^{-1}), glacial lakes with a size of less than 0.16 km^2 occupied more than 30% of total area (Table A3). Especially for the region in Nyainqentanglha, the area of small glacial lakes ($\leqslant$0.16 km^2) even accounts for 69.47% of the total area.

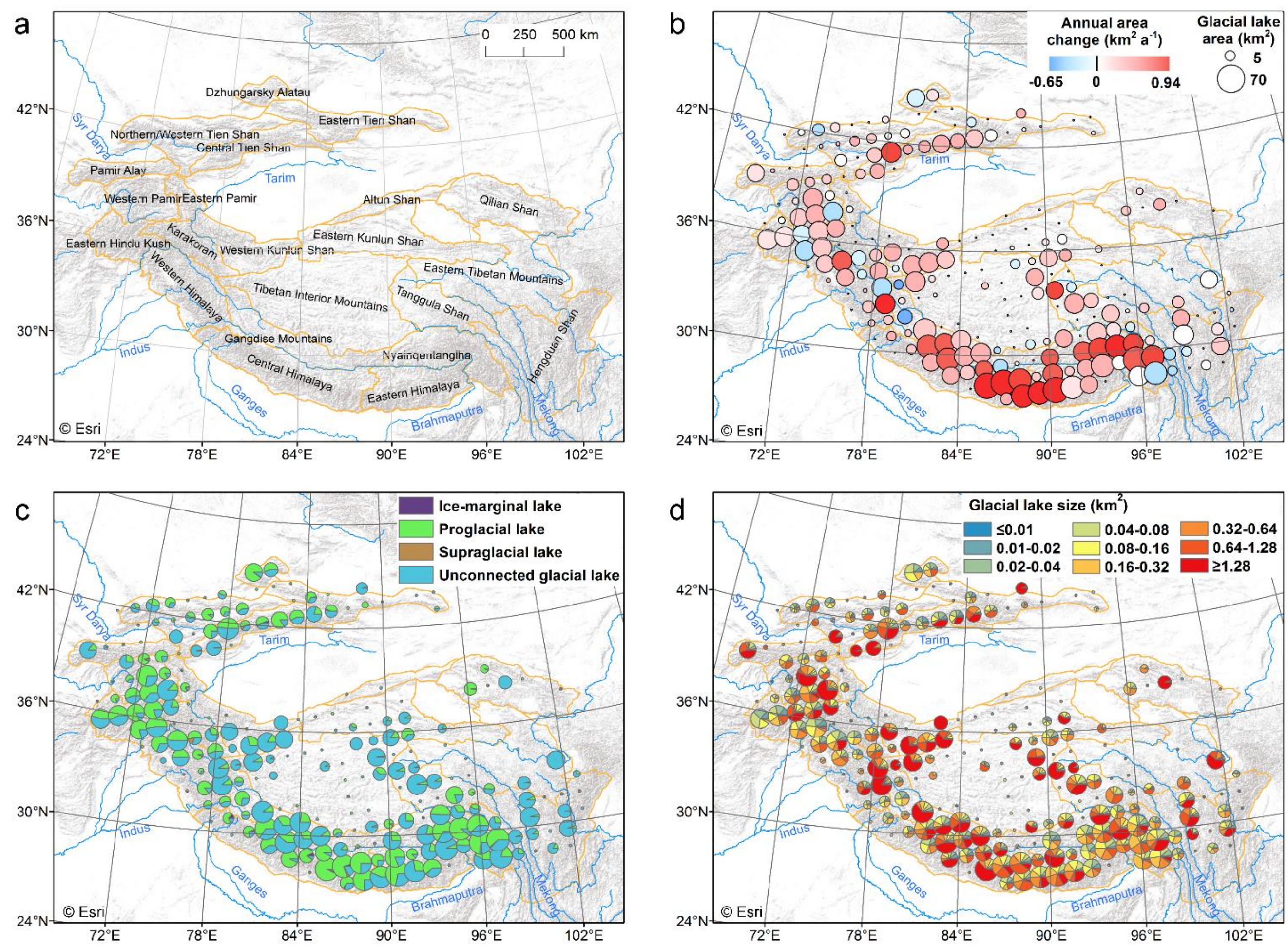

Fig. 6. Glacial lake area changes and area distribution. (a) Geographic coverage of mountain ranges in HMA. **(b)** Annual rate of change in lake area (2008-2017) on a 1°×1° grid. The size of the circle for the area in 2017. **(c)** Proportional areas of four types of glacial lakes in 2017. **(d)** Area of different sizes of glacial lakes in 2017. The terrain basemap is sourced from Esri (© Esri).

5.2 Influencing factors of current distribution of glacial lakes

To explore potential factors that have influenced glacial lake distribution across HMA, we focus on proglacial and supraglacial lakes, for which the changes are closely related with glaciers and expansion is most rapid. Proglacial lakes frequently develop from the enlargement and coalescence of one or more supraglacial lakes (Haritashya et al., 2018;Thakuri et al., 2016). Proglacial and supraglacial lake development from 2008 to 2017 is significantly correlated to initial lake area in 2008 (R=0.82, Table A4); larger ice-contact proglacial lakes imply a larger water body in contact with the calving-front of the glacier, and more rapid retreat (Truffer and Motyka, 2016;King et al., 2019).

For the years before 2008, the year-round Landsat 5 TM data in many years do not fully cover the HMA region. In this study we constructed the inventory over a ten-year time period, which is shorter than typical glacier response times which start from a minimum of 10 years for short, steep glaciers, to over 150 years for long debris-covered glaciers (Scherler et al., 2011). Hence, lake expansion is not expected to couple with short-term climate trends, particularly for debris covered glaciers (Haritashya et al., 2018). In the inclusion of mass balance forcing of glacial lake changes, the same questions about the response times also occur. Hence, rather than focus on the short term evolution of lake expansion, we investigated if climate and other factors have influenced the overall distribution of lake area, as observed in 2017. To investigate factors influencing the predominance of proglacial and supraglacial lakes, geomorphic, topographic and climate parameters were correlated with lake area over a 1°×1° grid, and aggregated (mean or summed) for HMA regions. A statistically significant positive correlation exists between lake area and debris-covered glacial area (after Scherler et al. 2018) across HMA (R=0.36, Table A4), confirming the predominance of pro- and supraglacial lakes forming on debris covered glacier tongues (Nie et al. 2017). Correlations and significance levels strengthen if the Karakoram is excluded (Table A5). The Karakoram is known as an anomaly of positive glacier mass balances and glacier advances (Gardelle et al., 2012) and also has an anomalously small area of proglacial lakes. Glacier length (RGI-Consortium, 2017) and debris cover are strongly correlated (R=0.85, Table A4), reflecting abundant debris on most large, low-gradient valley glacier tongues in HMA; in turn, there is a statistically significant direct correlation between glacier length and lake area (R=0.32, Table A4), as these tongues provide the ideal conditions for the coalescence of supraglacial ponds and formation of large proglacial lakes (Shaun D and John M, 2000;Nie et al., 2017). Glaciers are generally longest and most heavily debris covered in the Hindu Kush-Himalaya (Fig. 7a and Fig. 7b).

Some regions have comparable amounts of large debris-covered glaciers but substantial differences in total lake area and area-growth rates (for example, Central Himalaya compared to Central Tian Shan or Western Pamir, Table A5) . Regional differences in multi-decadal climate trends could play a role, with Nyainqentanglha, Central and Eastern Himalayan regions all characterized by rapid warming and decreased precipitation since 1979 (Fig. 7c and Fig. 7d), favoring negative glacial mass balances (Brun et al., 2017a). This plausibly explains why lake area is typically larger in these regions relative to adjacent regions further to the west and north (e.g. Western Himalaya) despite often similar glacier characteristics (in terms of debris cover and glacier length) (Fig. 7e and Fig. 7f). Further, there is very little debris covered area but rapid warming in Eastern Himalaya, where proglacial lakes are abundant (Fig. 7f). These results emphasize that the distribution of supra and proglacial lakes across HMA are primarily associated with the presence of large debris covered glaciers, but regional variability in warming and precipitation trends over the past few decades have likely also had some influence (Haritashya et al., 2018;Scherler et al., 2018;Dan and CLAGUE, 2011;Bo et al., 2019). These results are consistent with previous findings at regional scales, that have demonstrated a rapid expansion of proglacial lakes on debris-covered glaciers, with expansion in the upstream direction demonstrated to occur primarily through a process of subsidence at of the lake-contact debris covered glacier tongue (Harrison et al., 2018;Song et al., 2016;Song et al., 2017a).

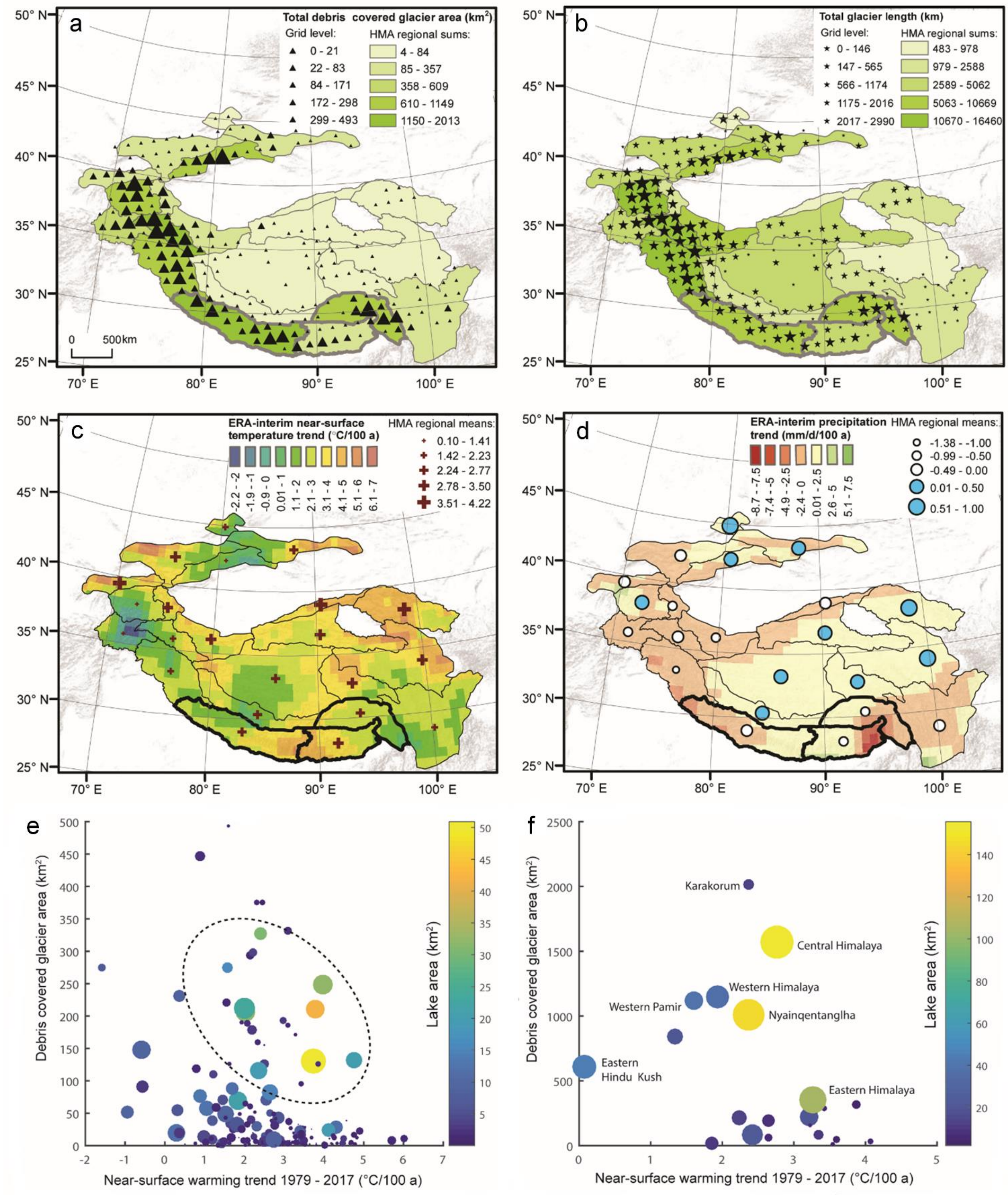

Fig. 7. Geomorphic and climatic influences on lake distribution. (a) Debris-covered area and **(b)** glacier length aggregated on a 1°×1° grid. Linear trends in **(c)** temperature and **(d)** precipitation calculated for 1979-2017 from ERA-Interim, including aggregated means over HMA regions. Relationship between total debris-covered area, near-surface temperature warming, and proglacial and supraglacial lake area of 2017 in **(e)** 1°×1° grid tiles and **(f)** HMA regions. Some regions discussed in the text are labelled. The lake coverage is high in areas of both rapid warming and high debris cover (E, dashed ellipse). Dot sizes are proportional to lake number. See Table A4 for details on data sources.

6 Discussions

6.1 Comparison with other lake datasets

We compared our dataset with that of Wang et al., 2020 for the closest period (2017 from Hi-MAG database and 2018 from Wang et al. 2020) over the spatial extent of our HMA region. The differences in the total number and area between these two dataset are 6206 and 223.97 km^2, respectively. We also found that 2077 glacial lakes with a total area of 178.77km^2 in our Hi-MAG dataset were not detected by Wang et al. The main reasons for the missed glacial lakes in Hi-MAG are because the interference of some bad observations (cloud or snow), glacial lake dried up or outburst, or located in the middle of the river.

To test the spatial correlation of glacial lakes distribution in two datasets, we compared the statistics in glacial lake number and area aggregated on a 0.1°×0.1° grid for the HMA regions. The results for the total glacial lake area, areas for glacial lakes larger than 0.04km^2, and number for glacial lakes larger than 0.04km^2 are depicted in Fig. A4. A clear and strong correlation can be observed for all the statistics between Hi-MAG dataset and glacial lake data by Wang et al. Most of the points being distributed around the 1:1 line, which shows that there is great consistency in the results.

In order to quantitatively and systematically evaluate the accuracy of our product, we implemented a stratified random sampling (Song et al., 2017b;Stehman and SV, 2012), where the glacial lakes were divided into four strata. The sample sizes are the spatial resolution (30 m) of the data, and the strata are designed as: C0W0. both the results are non glacial lakes; C0W1. non glacial lake for Chen's and glacial lake for Wang's; C1W0. glacial lake for Chen's and non glacial lake for Wang's; C1W1. Both the results are glacial lakes.

A total of 4,000 points were randomly selected, as shown in Fig. A5. The sample number for C1W1 and C1W0 are 1300 and 700, respectively, which is almost the same ratio between the total areas for the two strata (1450.50 km^2 vs 732.77 km^2). Because of the approximate total area with C1W0, we also randomly selected 700 samples from stratum C0W1. The rest 1300 samples are from C0W0. Every validation sample was visually examined using Landsat imagery and higher-resolution imagery in Google Earth. Sample pixels were interpreted by a regional glacial lake mapping expert, and ambiguous samples were cross-validated by a second observer. If a sample is difficult to interpret, it was marked as ambiguous sample and excluded for the accuracy assessment. The sample number estimates were produced for each of the four strata (Table A6), and these strata totals were then summed to obtain the total accuracy.

For the 1300 pixel samples that were considered to be non glacial lakes by both datasets, after the pixel by pixel verification, 1215 were indeed non glacial lakes, while 37 were the missed glacial lakes. In contrary, 1260 out of 1300 pixels belongs to the class of glacial lake, and 25 pixels were misclassified as glacial lakes by the two inventories. 307 error pixels were found in the results from Wang et al., constitute about half of the total validation number. For the glacial lakes identified only by our inventory, 678 out of 700 were corrected classified. Our results yielded high overall classification accuracy (88%), user's accuracy (97%), and producer's accuracy (82%) for glacial lake classification using Landsat data.

Hi-MAG was also compared with other Landsat-based lake inventories (Nie et al., 2017;Zhang et al., 2015;Pekel et al., 2016a). Hi-MAG lake number was 7268 higher and area was 644.26 km^2 higher than the estimation for the Tibetan Plateau (Zhang et al., 2015). The largest discrepancy is in the Gangdise, Himalaya and Nyainqentanglha Mountains in 2010. Across the Himalaya, we found 476.09 km^2 of glacial lakes, 4.57% more than previous estimates in 2015 (Nie et al., 2017). In addition, we qualitatively compared the lake extent between publicly available high-resolution Global Surface Water (GSW) dataset and our Hi-MAG database summed by mountain range in 2015. GSW data can be accessed at https://global-surface-water.appspot.com/download. For the sake of a reliable comparative analysis, lake polygons in the Hi-MAG dataset were converted into the grid format, and glacial lakes in the GSW were further extracted using the range of glacier buffer (10 km). Hi-MAG detected more glacial lakes in the Himalaya, Eastern Hindu Kush, and Tien Shan, and fewer in Eastern Pamir and Western Kunlun Shan. Fig. A6 illustrates the differences between our Hi-MAG glacial lake results and GSW-derived lake area for the whole HMA region.

The glacial lake area observed in our lake dataset in the Eastern Pamir and Western Kunlun Mountains does not conform to the mapped surface water in the GSW for these sub-regions. While there are numerous glacial lakes from an open water perspective, actually part of them are river segments. Additionally, the Himalaya, Eastern Hindu Kush, and some other Tien Shan host thousands of glacial lakes that are not readily observable in the GSW product. Large discrepancies in mountainous glacial lake estimates preclude a significant consistency between GSW and our Hi-MAG lake data over the HMA region. The region with the highest consistency between GSW and Hi-MAG product is interior Tibet. There is little agreement for Tien Shan, where the weather is rainy and snowy in the region above 3000 m, and large amounts of ancient glacial deposits have been accumulated. Here glacial lakes are featured by small size, due to the influence of source glaciers and lake beds, as well as the water depth and sediment inflow, glacial lakes appear heterogeneous reflectance in the image. Errors could exist in datasets produced by automated classification, but we also did a detailed manual editing, so we were not relying exclusively on automatic classification. Karakoram regions seem to have fewer glacial lakes in our estimate, owing to the overestimation of surface water on debris covered glaciers in the GSW dataset.

The little agreement between our Hi-MAG glacial lakes data and GSW data is mainly due to its lack of systematic glacial lake inventories and mapping capabilities. The lake dynamics and differing climate contexts within HMA may also lead to inconsistencies between the sub-regions. Hi-MAG might have made better use of the optimum satellite imaging season to map glacial lakes, potentially resulting in more complete mapping by avoiding conditions — such as periods of lake ice — that may confound mapping.

6.2 Known issues and planned improvements

There are several important issues and limitations to the datasets produced and methods used within this study that are important to highlight to potential users. (i) Bodies of water smaller than nine connected pixels (e.g., 1 x 9 pixels or 3 x 3 pixels, corresponding to 30 x 270 m or 90 x 90 m, respectively), those obscured by frozen water surface and loose moraines or hidden by terrain shadows were not included. Broken floating ice or isolated moraine that stand in open water for some times were mapped. Supraglacial lakes such as melt ponds developed on the surface of glaciers present particular challenges because of their small size and highly dynamic properties. Most supraglacial lakes are transient or seasonal, or at least fluctuate seasonally, as they commonly drain and may refill, but in fact this short-duration seasonal water more generally is likely to be underestimated because of temporal discontinuities in the archive and gaps caused by persistent cloud cover. (ii) The spatial and temporal information reported in the Landsat dataset used in this study complements that acquired in the past.

Nevertheless, the biggest limitation to glacial lake mapping from these data are undoubtedly the geographic and temporal discontinuities of the Landsat archive itself. Historical data over the entire HMA before 2008 can be recovered partly from the Landsat 4 TM/MSS, Landsat 5 TM, Landsat 7 ETM+, and partly from SPOT, and other satellite systems, etc., although data access is not always at the full, free and open level of Landsat. In this regard, ASTER is freely accessible and has higher resolution than Landsat, but the temporal coverage is very limited in most of HMA. Other Landsat-like moderate resolution multi-spectral sources could be also used to improve and extend the temporal sampling. For example the European Space Agency's Sentinel 2a satellite launched in 2015 and provides optical imagery at 10 m resolution (Wang et al., 2020a), which will benefit future research combing all available satellite observations with GEE cloud computing power would make long-term monitoring of changes to HMA's glacial lakes and inland waters possible.

7 Data availability

The Hi-MAG database is distributed under a Creative Commons Attribution 4.0 License. The data can be downloaded from the data repository Zenodo at https://doi.org/10.5281/zenodo.4059181 (Chen et al., 2020).

8 Conclusions

In conclusion, the Hi-MAG dataset and others have turned to Earth observation satellite data, especially Landsat imagery, to provide a more consistent delineation of large-scale glacial lake changes. Some remote-sensed glacial lake mapping methods have enabled local-scale area estimation or spatial representation of lake extent and change. Such methods result in relatively good performance for lake areas that remain clear and show homogeneous reflectance in the image, but do not allow for continental-scale glacial lake mapping that have spectral interference from the other objects such as glaciers, snow, clouds, turbidity and sedimentation characteristics of glacial lake itself, or the atmospheric interference and terrain effects. Automated methods for the extraction of glacial lakes over the large-scale areas are further developed in our work. However, visual interpretation and manual editing is still an effective way to ensure the high accuracy of lake inventories and appended attributed information for further analysis. Based on an error of ±1 pixels on the lake boundary, the area uncertainty of each glacial lake ranged from 0.30% to 50% for the year between 2008 and 2017, and the mean area uncertainty of 17% in the entire HMA region.

Mapping of glacial lakes across the Tibetan Plateau and adjoining ranges reveals a complex pattern of lake occurrence and growth/shrinkage. During the past ten years, 2755 glacial lakes with a total area of 90.14 km^2 were increased in the HMA region. Proglacial lakes contributed 62.87% of that increase. We found that most of areas in HMA have experienced rapid expansions, Central and Eastern Himalaya, Central Tien Shan showed the most lake area increases (up to +0.94 km^2 a^{-1}). Negative area changes were observed in the Eastern Tien Shan, Eastern Hindu Kush, Hengduan Shan and Eastern Tibetan Mountains. The number of lakes grown very rapidly above 4400 m a.s.l. Proglacial lake growth is proceeding at high elevations of above 4900 m, but glacier retreat and lake disconnections are also starting to occur at higher elevations, causing the number and area of both classes to increase. At low elevations, few glaciers remain where proglacial lakes can form, and already detached lakes lack growth mechanisms. Overall, continued growth of glacial lakes can be expected, particularly where large debris covered tongues remain.

This freely-downloadable, detailed Hi-MAG dataset can also be used in future studies to provide a sound and consistent basis on which to quantify critical relationships and processes in HMA, including glacier-climate-lake interactions, glacio-hydrologic models, glacial lake outburst floods and potential downstream risks and water resources.

Appendix A

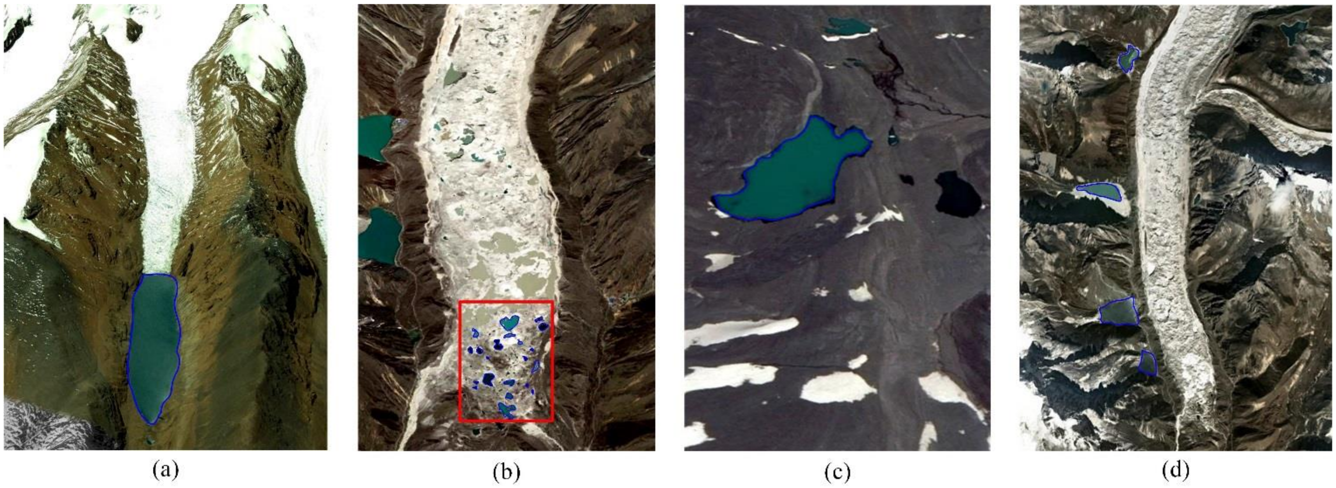

Fig. A1. Examples of the various types of glacial lake found in the HMA: (a) pro-glacial lakes, which are connected to the parent glacier and usually impounded by a debris dam (usually a moraine or ice-cored moraine); (b) supraglacial lakes (denoted by the red rectangle) which develop on the glacier surface; (c) unconnected glacial lakes; and (d) ice-marginal lakes that distributed on the edge of a glacier. Background images were acquired from © Google Earth, and were shot in 2009, 2011, 2012 and 2014, respectively. Glacial lake outlines for each type are shown in blue color.

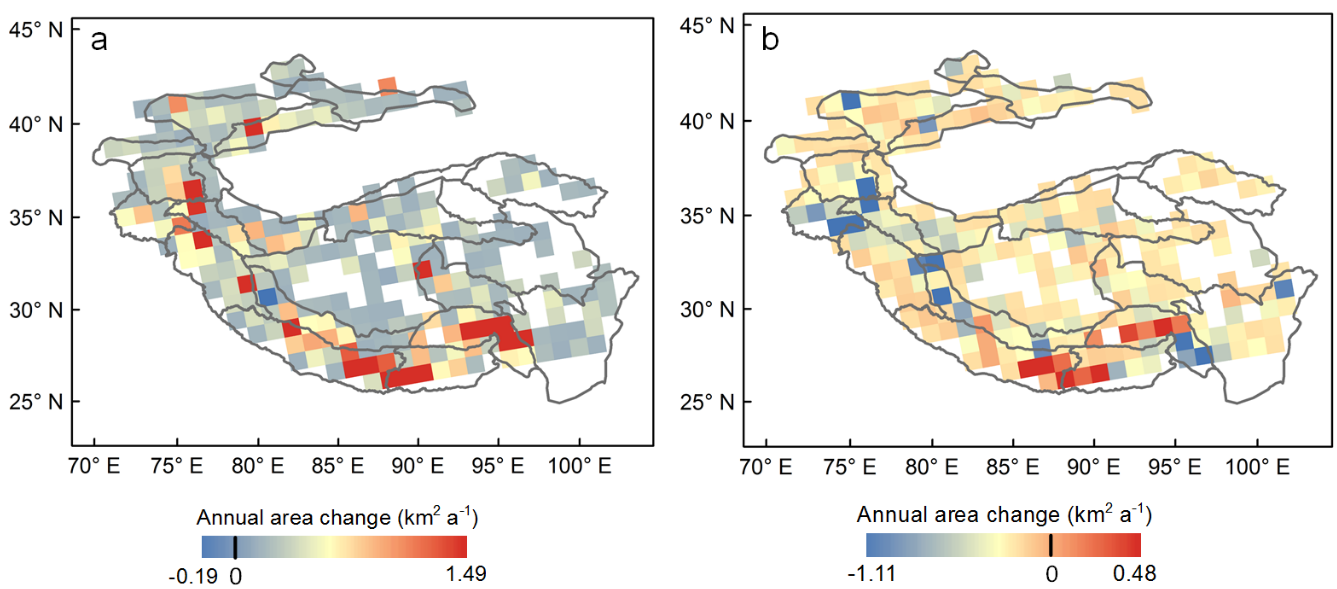

Fig. A2. Annual changes in lake area between 2008 and 2017 on a 1°×1° grid. The (a) upper and (b) lower slopes represent the 90% confidence interval.

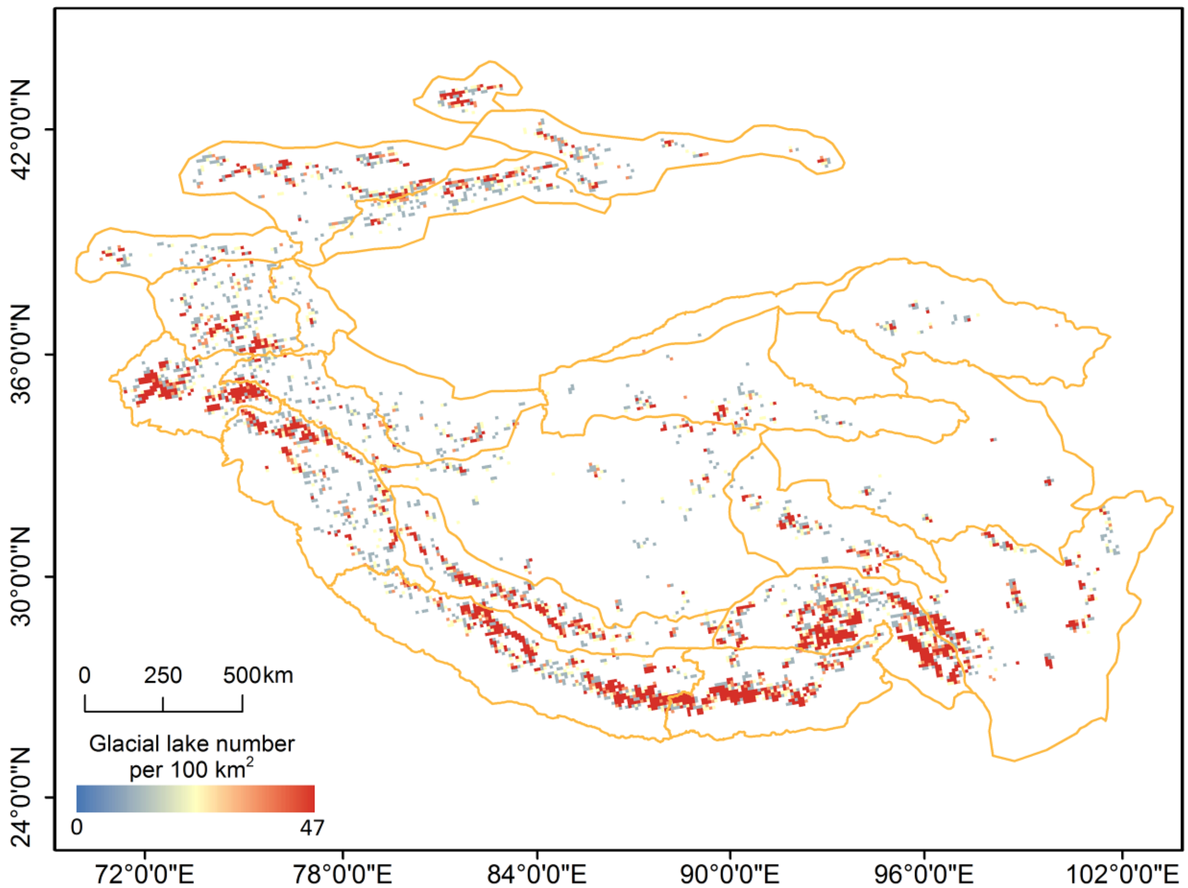

Fig. A3. Density (number per 100 km^2) distribution of glacial lakes in 2017.

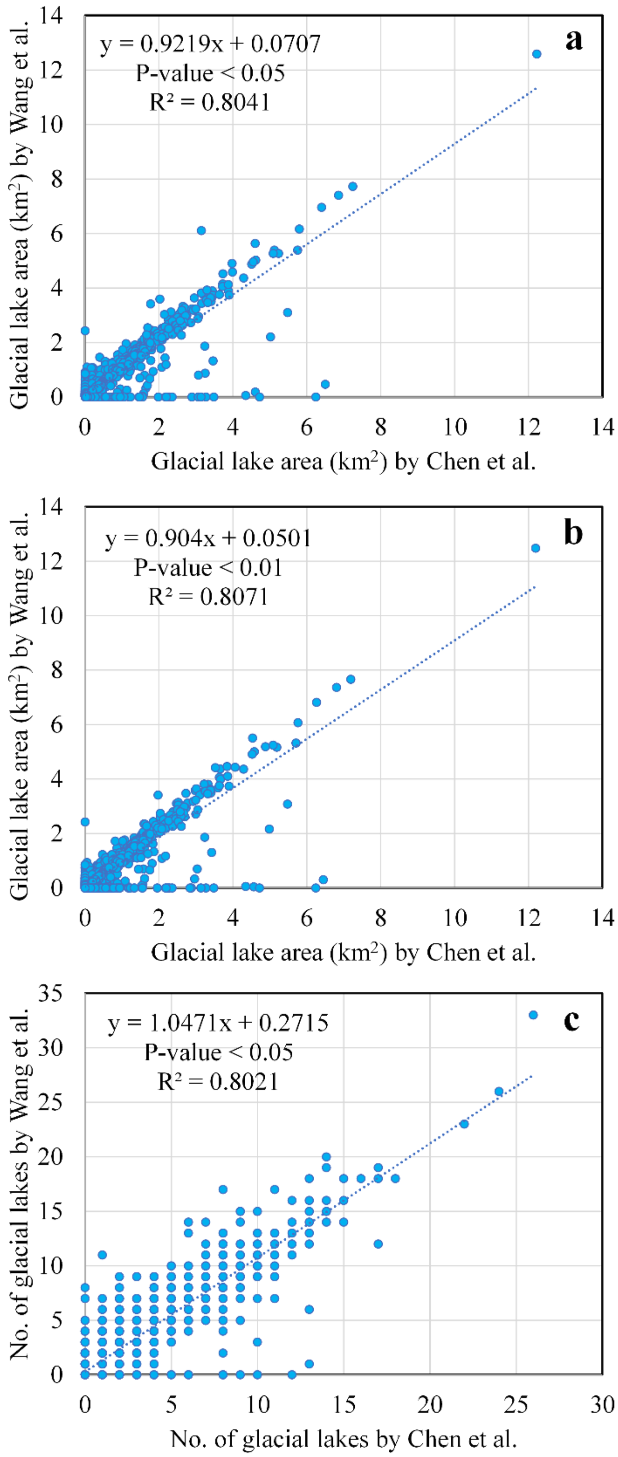

Fig. A4. Comparison the results of (a) total glacial lake area, (b) areas for glacial lakes larger than 0.04km^2, and (c) number for glacial lakes larger than 0.04km^2 summed over a 0.1°×0.1° grid between Hi-MAG database and inventory by Wang et al., 2020.

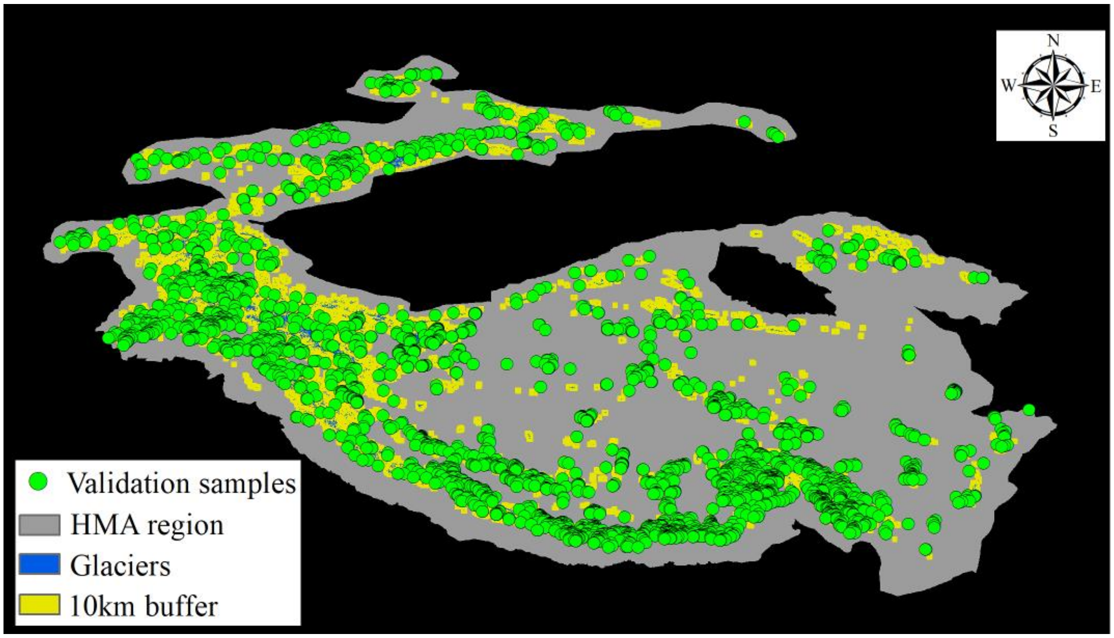

Fig. A5. Distribution of validation samples selected using stratified random sampling. Blue polygons are glacier outlines taken from the Randolph Glacier Inventory (RGI v5.0), the Second Chinese Glacier Inventory (CGI2) and the GAMDAM inventory. Yellow polygons refer to buffer area within 10 km of glacier terminals.

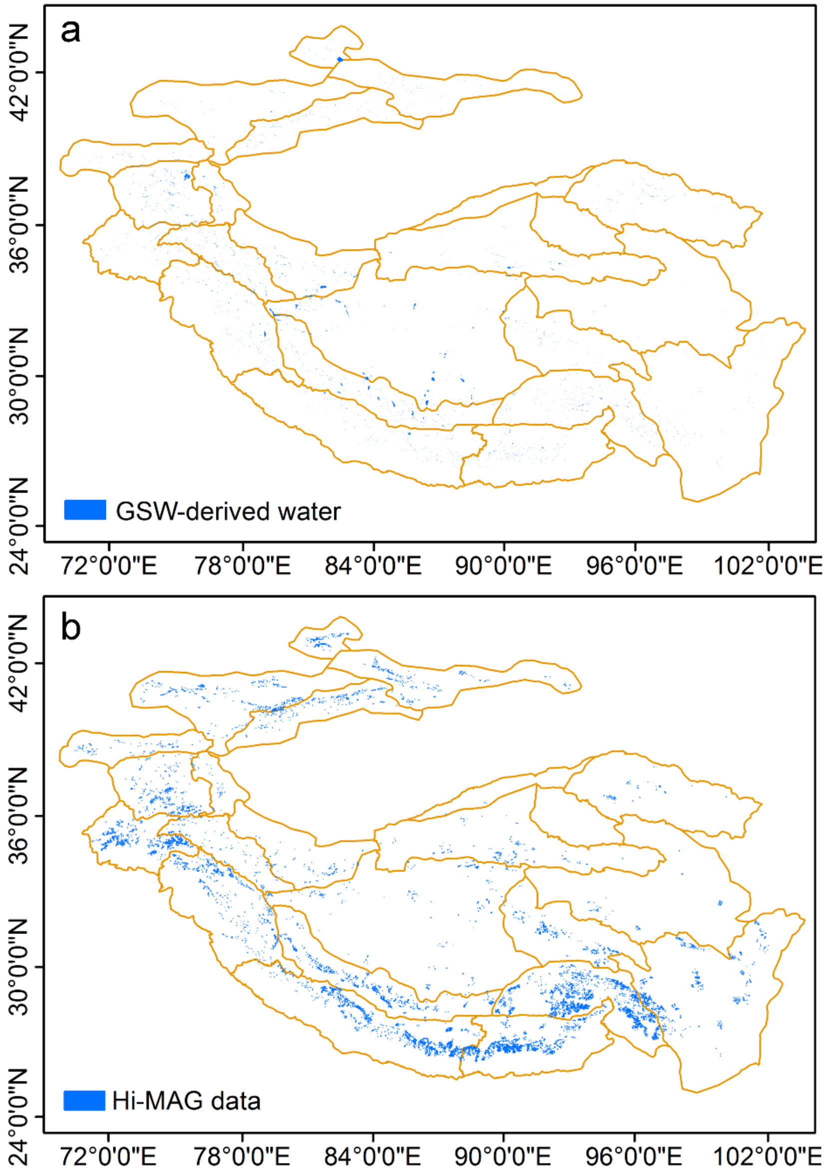

505 **Fig. A6. Comparison of the glacial lake measured in the global maps of (a) Pekel et al. and (b) our Hi-MAG data.**

Table A1. Mountain-wide glacial lake number and area per year and total loss/gain from 2008 to 2017. The unit of area is km^2.

Mountain range	2008		2009		2010		2011		2012		2013		2014		2015		2016		2017		Total gain/loss (2008-2017)	
	No.	Area	No.	Area	No.	Area	No.	Area	No.	Area	No.	Area	No.	Area	No.	Area	No.	Area	No.	Area	No.	Area
Eastern Hindu Kush	1227	73.63	856	61.40	1113	68.91	1036	67.94	1015	59.80	1206	67.90	1179	71.30	1172	66.36	1260	65.77	1399	70.83	172	-2.80
Western Himalaya	894	77.65	856	70.23	756	71.25	747	71.38	746	68.95	779	76.00	874	82.76	823	78.33	999	79.51	1005	87.96	111	10.31
Eastern Himalaya	1634	164.12	1667	163.10	1675	166.49	1836	172.87	1859	171.67	1910	176.54	1943	174.93	2159	190.96	1954	179.09	1943	179.80	309	15.68
Central Himalaya	1312	182.54	1697	179.04	1577	188.35	1847	195.77	1782	195.56	1728	196.72	1850	198.52	2049	206.80	2096	206.41	2182	209.63	870	27.09
Karakoram	167	18.89	214	16.78	206	17.91	159	14.90	152	13.55	182	14.76	163	15.41	182	17.02	250	18.26	219	18.60	52	-0.29
Western Pamir	481	75.53	486	77.64	526	83.27	548	80.86	495	79.17	537	79.32	550	81.20	557	83.96	570	81.76	624	75.82	143	0.29
Eastern Pamir	38	5.06	45	5.69	48	5.81	43	4.99	56	5.75	50	5.43	50	5.26	49	5.65	58	5.66	56	5.81	18	0.75
Pamir Alay	124	10.82	79	9.76	100	10.93	132	11.79	129	11.60	127	11.74	128	11.66	137	11.79	130	11.54	131	12.10	7	1.28
Northern/Western Tien Shan	474	36.16	358	37.20	499	36.87	541	41.71	522	36.04	518	36.98	551	46.06	530	38.28	512	37.38	626	40.91	152	4.75
Central Tien Shan	307	29.19	241	29.43	305	32.65	334	35.44	340	35.41	335	32.36	333	36.07	337	35.51	441	35.97	471	36.69	164	7.50
Eastern Tien Shan	247	15.83	230	17.24	241	15.99	245	15.64	251	15.75	259	16.15	250	16.07	297	17.31	241	17.99	245	18.31	-2	2.48
Western Kunlun Shan	112	40.27	134	38.30	121	36.92	119	41.41	111	39.84	136	37.09	108	37.62	120	41.62	126	40.54	132	44.71	20	4.44
Eastern Kunlun Shan	180	11.92	193	12.83	265	20.62	237	16.46	232	15.74	246	15.90	244	16.72	290	18.49	255	17.95	248	16.90	68	4.98
Gangdise Mountains	852	99.15	908	96.46	848	104.24	886	96.88	961	102.48	895	95.75	954	96.28	991	94.64	1053	96.37	1116	99.83	264	0.68
Hengduan Shan	909	62.25	1077	64.70	967	65.38	867	61.29	927	62.75	1064	66.53	948	63.82	1023	65.45	942	62.93	961	63.35	52	1.10
Tibetan Interior Mountains	335	52.96	308	44.76	349	47.59	334	46.42	318	46.94	334	47.73	313	46.17	335	48.12	318	44.74	315	47.97	-20	-4.99
Eastern Tibetan Mountains	57	12.74	86	13.74	86	14.39	107	15.38	84	13.65	100	14.35	93	14.93	76	13.58	85	14.53	66	13.60	9	0.86
Tanggula Shan	468	39.45	318	40.99	344	44.28	327	43.24	347	42.17	363	43.40	376	44.97	461	45.53	372	45.94	363	44.97	-105	5.52
Qilian Shan	82	7.96	78	8.67	91	9.68	77	9.23	76	9.19	85	9.36	90	10.38	86	9.90	80	9.99	67	8.97	-15	1.01
Dzhungarsky Alatau	290	13.82	218	11.57	233	11.75	272	12.60	259	12.48	269	12.68	267	12.90	205	11.80	240	12.44	264	12.80	-26	-1.02

Nyainqentanglha	2401	275.33	2647	255.23	2614	272.95	2539	273.28	2594	266.60	2856	275.46	2646	277.70	2977	280.35	2660	292.24	2911	285.68	510	10.35

Table A2. Mountain-wide annual glacial lake area from 2008 to 2017 for proglacial lakes and unconnected lakes. Supraglacial and ice-marginal lakes have relative few coverage areas and are not listed details in the table. The unit of area is km^2. Acronyms are used to represent the name of mountain ranges to save space.

		EHK	WH	EH	CH	K	WP	EP	PA	N/WT	CT	ET	WK	EK	G	H	TIM	ETM	T	Q	DA	N	Total
Proglacial lakes	2008	46.71	34.58	91.45	133.06	10.99	34.07	4.56	4.13	17.77	14.52	9.12	5.15	1.58	24.01	11.40	3.59	0.76	9.73	3.74	11.19	133.29	605.40
	2009	37.98	30.03	92.97	130.09	10.60	34.27	5.30	2.79	16.39	14.07	8.11	5.69	1.72	19.97	12.58	2.97	1.54	10.12	4.71	9.04	122.95	573.90
	2010	41.68	29.73	95.11	137.49	10.55	35.72	5.02	3.57	18.09	16.70	9.18	5.73	5.66	22.27	13.55	4.72	1.68	11.52	5.25	9.24	136.04	618.48
	2011	42.77	32.88	100.58	143.53	9.70	34.82	4.62	4.04	20.27	15.64	8.66	4.73	3.69	20.76	12.14	3.80	1.74	10.63	4.71	10.18	136.69	626.59
	2012	37.32	31.30	99.54	143.02	9.00	34.87	5.12	3.91	18.58	16.76	8.83	4.69	3.66	21.78	12.83	3.73	1.74	10.60	4.66	10.02	133.29	615.25
	2013	41.67	30.58	100.97	141.25	9.22	34.57	4.71	4.08	18.28	16.72	9.20	4.95	3.51	20.56	13.55	3.99	1.67	10.60	4.74	10.07	136.58	621.47
	2014	43.88	36.12	98.12	145.22	9.96	35.06	4.71	4.15	20.33	17.37	8.88	5.04	4.40	21.88	12.91	4.38	1.75	10.68	5.01	10.21	136.95	637.00
	2015	40.49	33.88	108.45	151.17	10.68	37.63	5.03	4.02	18.98	16.26	9.53	5.08	5.01	22.66	13.53	4.44	1.62	11.30	4.67	9.43	138.12	652.00
	2016	40.52	34.20	103.31	150.59	10.92	36.13	5.02	3.83	18.12	17.63	8.31	4.67	4.03	23.29	13.03	4.08	1.74	10.75	4.73	9.99	147.83	652.73
	2017	43.53	35.52	103.75	152.52	11.33	37.60	5.16	4.03	20.07	18.56	8.52	5.36	4.21	23.31	13.59	4.41	1.69	10.49	4.71	10.15	143.58	662.07
Unconnected lakes	2008	26.82	41.86	70.98	43.82	6.33	41.24	0.47	6.70	18.38	14.56	6.69	35.10	10.35	74.83	50.60	49.08	11.98	29.50	4.23	2.57	140.42	686.53
	2009	23.35	39.37	69.41	45.41	4.81	43.00	0.39	6.98	20.79	15.36	9.07	32.56	11.07	76.41	52.10	41.80	12.21	30.87	3.97	2.49	131.63	673.04
	2010	27.08	40.69	70.78	46.96	5.64	47.24	0.80	7.37	18.78	15.87	6.79	31.20	14.81	81.97	51.83	42.87	12.71	32.76	4.44	2.49	136.12	699.22
	2011	25.00	37.62	71.65	47.79	4.44	45.79	0.31	7.75	21.42	19.76	6.96	36.65	12.78	76.13	49.16	42.63	13.64	32.59	4.52	2.34	136.05	694.98
	2012	22.41	36.80	71.23	47.75	3.74	44.13	0.50	7.69	17.44	18.48	6.82	35.15	12.04	80.71	49.92	43.22	11.92	31.53	4.54	2.37	132.53	680.92
	2013	26.10	44.59	74.81	50.85	4.09	44.52	0.59	7.67	18.68	15.55	6.83	32.09	12.34	75.20	52.98	43.75	12.69	32.77	4.62	2.51	138.07	701.31
	2014	27.27	45.69	75.92	48.65	4.31	45.85	0.43	7.52	25.69	18.54	7.08	32.55	12.29	74.40	50.92	41.74	13.19	34.26	5.38	2.60	140.03	714.33
	2015	25.76	43.60	81.11	50.30	5.76	46.08	0.47	7.76	19.29	19.15	7.66	36.54	13.44	71.98	51.92	43.66	11.96	34.20	5.23	2.30	141.40	719.59
	2016	25.14	44.34	74.76	50.30	6.06	45.39	0.49	7.70	19.24	17.77	9.57	35.81	13.91	73.09	49.91	40.66	12.79	35.15	5.26	2.35	143.38	713.11
	2017	27.19	51.42	74.96	51.59	6.54	37.95	0.46	8.06	20.81	17.52	9.66	39.34	12.68	76.53	49.76	43.57	11.91	34.45	4.27	2.56	141.22	722.44

Table A3. Area of different sizes of glacial lakes in 2017 for some regions with large area growth of rate. The unit of area is km^2.

Lake grid ID (Mountain ranges)	69 (N)	116 (CH)	274 (WH)	71 (N)	48 (H)	74 (N)	72 (N)	14 (EH)	13 (EH)	39 (CH)	15 (EH)
≤0.01km^2	0.18	0.28	0.20	0.16	0.22	0.16	0.17	0.23	0.16	0.32	0.33
0.01km^2-0.02km^2	0.85	1.51	1.29	0.71	1.43	1.08	1.37	1.45	1.45	1.49	2.46
0.02km^2-0.04km^2	1.69	2.16	2.22	1.79	3.24	2.09	2.29	2.24	2.06	2.72	4.14
0.04km^2-0.08km^2	1.78	3.19	2.98	2.20	5.30	3.38	4.45	2.77	2.69	3.66	7.16
0.08km^2-0.16km^2	1.91	5.38	3.87	2.86	4.81	4.03	5.06	3.75	4.33	5.00	13.16
0.16km^2-0.32km^2	1.81	4.53	2.23	2.76	4.62	5.55	5.81	2.91	3.90	5.66	11.62
0.32km^2-0.64km^2	1.01	5.37	1.77	1.79	3.88	1.75	3.81	5.72	3.99	7.13	12.37
0.64km^2-1.28km^2	0.00	2.94	0.00	1.38	2.82	2.96	4.43	0.96	7.10	8.97	7.74
≥1.28km^2	0.00	7.22	4.19	0.00	11.46	3.17	2.59	6.07	1.40	6.06	12.00
Total area (km^2)	9.22	32.58	18.76	13.66	37.76	24.17	29.99	26.10	27.09	41.00	70.96
Total area (≤0.16km^2)	6.41	12.52	10.57	7.72	14.99	10.74	13.35	10.45	10.69	13.18	27.24
% of Total area (≤0.16km^2)	69.47	38.43	56.32	56.56	39.70	44.45	44.52	40.03	39.47	32.15	38.39
Annual area increase (km^{2}a^{-1})	0.23	0.28	0.28	0.29	0.32	0.41	0.42	0.49	0.70	0.74	0.94

Table A4. Summary of correlation coefficients (*R*) for key lake, topographic, geomorphic and climatological parameters, calculated within 1°×1° grid cells across HMA. Correlation coefficients are bold where $p < 0.05$; (*) indicates $p < 0.01$.

	Lake area (2008)	Lake area (2017)	Lake change (2008 – 2017)	Glacier (gl.) area ^	Debris-covered gl. area	Total gl. length	Mean gl. slope	Mean gl. elevation	Temperature change^^ 1979 – 2017	Precipitation change 1979 – 2017
Lake area (2008)	1.00									
Lake area (2017)	**0.99***	1.00								
Lake change (2008 – 2017)	**0.82***	**0.87***	1.00							
Glacier (gl.) area	**0.23***	**0.24***	**0.22***	1.00						
Debris-covered gl. area	**0.35***	**0.36***	**0.34***	**0.85***	1.00					
Total gl. length	**0.32***	**0.32***	**0.28***	**0.90***	**0.85***	1.00				
Mean gl. Slope	0.07	0.07	0.05	0.02	**0.18**	0.06	1.00			
Mean gl. Elevation	0.12	0.14	**0.17**	0.11	0.00	0.05	**-0.28***	1.00		
Temperature change 1979 – 2017	-0.09	-0.07	0.10	**-0.17**	**-0.25***	**-0.27***	0.00	0.07	1.00	
Precipitation change	-0.03	-0.01	0.09	-0.13	**-0.16**	**-0.15**	**-0.18***	**0.15**	**0.16**	1.00

^ Glacier data is derived from the Randolph Glacier Inventory (RGI Consortium, 2017), except for debris cover (after Scherler et al. 2018). Climate data is for ERA Interim

^^ ERA-Interim near surface temperature and precipitation fields for the period 1979 – 2017 were obtained from the KNMI climate explorer (https://climexp.knmi.nl).

Table A5. Regional summary of key topographic, geomorphic and climatological parameters compared to pro- and supraglacial lake area in 2017. Correlation coefficients are bold where *p* < 0.05; (*) indicates *p* < 0.01.

Region	Total area (km^2)	Lake area (km^2)	Glacier (gl.) area (km^2)	Debris-covered gl. area (km^2)	Total gl. length (km)	Mean gl. slope (°)	Mean gl. elevation (m)	Temperature change 1979 – 2017 (°C/century)	Precipitation change 1979 – 2017
Central Himalaya	254886	155.7	8678	1567	10669	26	5542	2.77	-0.25
Central Tien Shan	105456	19.0	7270	842	7415	27	4181	1.35	0.05
Dzhungarsky Alatau	37542	10.3	521	18	978	24	3615	1.85	0.74
Eastern Himalaya	164785	104.7	2838	357	3614	24	5484	3.26	-0.84
Eastern Hindu Kush	95404	43.6	2938	609	5062	25	4856	0.08	-0.86
Eastern Kunlun Shan	256729	4.2	2995	45	3384	24	5389	3.60	0.06
Eastern Pamir	39605	5.2	2118	291	2364	27	5064	3.42	-0.50
Eastern Tibetan Mountains	333123	1.8	312	12	483	24	5345	3.55	0.73
Eastern Tien Shan	140900	8.7	2332	193	3977	28	3974	2.65	0.17
Gangdise Mountains	154884	23.2	1271	80	2570	24	5892	2.42	0.33
Hengduan Shan	372649	13.6	1281	212	2048	23	5278	2.24	-0.13
Karakoram	83644	11.7	21474	2013	16460	31	5399	2.37	-0.35
Northern/Western Tien Shan	187275	20.1	2262	223	4138	23	3943	3.22	-0.36

Nyainqentanglha	172746	144.6	7047	1011	8710	25	5282	2.37	-1.00
Pamir Alay	71845	4.0	1847	319	3441	25	4109	3.88	-0.27
Qilian Shan	201699	4.7	1598	30	2588	26	4847	4.07	0.51
Tanggula Shan	145064	10.6	1841	84	1893	21	5521	3.34	0.46
Tibetan Interior Mountains	526111	4.4	3815	59	4179	23	5927	2.64	0.31
Western Himalaya	189494	36.3	7986	1149	11974	24	5180	1.93	-1.24
Western Kunlun Shan	123388	5.3	8457	159	8108	26	5642	3.22	-0.55
Western Pamir	109239	37.9	8417	1118	11640	27	4844	1.61	0.08
Lake area: Correlation Coefficient (*R*)			0.21	**0.50**	0.36	0.01	0.23	-0.17	**-0.49**
Exl. Karakoram			**0.49**	**0.72***	**0.52**	0.10	0.25	-0.18	**-0.50**

Table A6. Statistical results of stratified random sampling.

Strata	Total pixel number	Total area (km^2)	Sample number	Sample No. of non glacial lake	Sample No. of glacial lake	No. of ambiguous sample
C0W0	2,022,448,650	1,820,203.78	1300	1215	37	48
C0W1	925,449	832.90	700	307	362	31
C1W0	814,196	732.77	700	21	678	1
C1W1	1,611,668	1,450.50	1300	25	1260	15

Author contributions. FC: conceptualization, methodology, lake evolution analysis, project administration, resources, and writing; MMZ: conceptualization, methodology, lake evolution analysis, validation, and writing; HDG: funding acquisition, supervision, and writing; SA: methodology, climate and debris cover analysis, validation, and writing; JSK: analysis, interpretation, and writing; UH: writing and interpretation; CSW: writing.

Competing interests. The authors declare that they have no conflict of interest.

Acknowledgements. We thank T Bolch, and D Shugar for their contributions to this project in its stages of development; L Wang, SG Xu, ZY Lin, H Zhao, YHZ He, TC Shan, ZW Xu, N Wang, ZZ Yin, and JX Wang for cross-validation of data that were so integral to this project.

Financial support. This work was supported by the Strategic Priority Research Program of the Chinese Academy of Sciences (XDA19030101), the International Partnership Program of the Chinese Academy of Sciences (131211KYSB20170046/131C11KYSB20160061), and the National Natural Science Foundation of China (41871345). SA was supported by the EVOGLAC project under the Swiss National Science Foundation (IZLCZ2_169979/1).

References

Aggarwal, S., Rai, S. C., Thakur, P. K., and Emmer, A.: Inventory and recently increasing GLOF susceptibility of glacial lakes in Sikkim, Eastern Himalaya, Geomorphology, 295, 39-54, https://doi.org/10.1016/j.geomorph.2017.06.014, 2017.

Armstrong, W. H., and Anderson, R. S.: Ice-marginal lake hydrology and the seasonal dynamical evolution of Kennicott Glacier, Alaska, Journal of Glaciology, 1-15, 2020.

Ashraf, A., Naz, R., and Roohi, R.: Glacial lake outburst flood hazards in Hindukush, Karakoram and Himalayan Ranges of Pakistan: implications and risk analysis, Geomatics, Natural Hazards and Risk, 3, 113-132, 10.1080/19475705.2011.615344, 2012.

Baumann, F., Jinsheng, H. E., Karsten, S., Peter, K., and Thomas, S.: Pedogenesis, permafrost, and soil moisture as controlling factors for soil nitrogen and carbon contents across the Tibetan Plateau, Global Change Biology, 15, 3001–3017, 2009.

Bhardwaj, A., Singh, M. K., Joshi, P. K., Snehmani, Singh, S., Sam, L., R.D.Gupta, and RajeshKumar: A lake detection algorithm (LDA) using Landsat 8 data: A comparative approach in glacial environment, International Journal of Applied Earth Observations & Geoinformation, 38, 150-163, 2015.

Bo, Zhao, Yunsheng, Wang, Yonghong, Luo, Ruifeng, Liang, Jia, and Li: Large landslides at the northeastern margin of the Bayan Har Block, Tibetan Plateau, China, Royal Society Open Science, 6, 180844, 2019.

Bolch, T., Kulkarni, A., Kääb, A., Huggel, C., Paul, F., Cogley, J. G., Frey, H., Kargel, J. S., Fujita, K., and Scheel, M.: The state and fate of Himalayan glaciers, Science, 336, 310, 2012a.

Bolch, T., Kulkarni, A., Kaab, A., Huggel, C., Paul, F., Cogley, J. G., Frey, H., Kargel, J. S., Fujita, K., and Scheel, M.: The State and Fate of Himalayan Glaciers, Science, 336, 310-314, 2012b.

Brun, F., Berthier, E., Wagnon, P., Kääb, A., and Treichler, D.: A spatially resolved estimate of High Mountain Asia glacier mass balances from 2000 to 2016, Nature Geoscience, 10, 668-673, 2017a.

Brun, F., Berthier, E., Wagnon, P., Kaab, A., and Treichler, D.: A spatially resolved estimate of High Mountain Asia glacier mass balances from 2000 to 2016, Nature Geoscience, 10, 668-673, 2017b.

Capps, D. M., Wiles, G. C., Clague, J. J., and Luckman, B. H.: Tree-ring dating of the nineteenth-century advance of Brady Glacier and the evolution of two ice-marginal lakes, Alaska, The Holocene, 21, 641-649, 2011.

Chen, F., Zhang, M., Tian, B., and Li, Z.: Extraction of Glacial Lake Outlines in Tibet Plateau Using Landsat 8 Imagery and Google Earth Engine, IEEE Journal of Selected Topics in Applied Earth Observations & Remote Sensing, 10, 4002-4009, 2017.

Chen, J., Zhu, X., E.Vogelmann, J., Gao, F., and Jin, S.: A simple and effective method for filling gaps in Landsat ETM+ SLC-off images, Remote Sensing of Environment, 115, 1053-1064, 2011.

Dan, H. S., and CLAGUE, J. J.: The sedimentology and geomorphology of rock avalanche deposits on glaciers, Sedimentology, 58, 1762-1783, 2011.

Gardelle, J., Berthier, E., and Arnaud, Y.: Slight mass gain of Karakoram glaciers in the early twenty-first century, Nature Geoscience, 5, 322-325, 10.1038/ngeo1450, 2012.

Gardelle, J., Berthier, E., Arnaud, Y., and Kääb, A.: Region-wide glacier mass balances over the Pamir-Karakoram-Himalaya during 1999–2011, The Cryosphere, 7, 1263-1286, 10.5194/tc-7-1263-2013, 2013.

Gardner, A. S., Moholdt, G., Cogley, J. G., Wouters, B., Arendt, A. A., Wahr, J., Berthier, E., Hock, R., Pfeffer, W. T., and Kaser, G.: A reconciled estimate of glacier contributions to sea level rise: 2003 to 2009, Science, 340, 852, 2013.

Hanqiu, X.: Modification of normalised difference water index (NDWI) to enhance open water features in remotely sensed imagery, International Journal of Remote Sensing, 27, 3025-3033, 2006.

Haritashya, U. K., Kargel, J. S., Shugar, D. H., Leonard, G. J., Strattman, K., Watson, C. S., Shean, D., Harrison, S., Mandli, K. T., and Regmi, D.: Evolution and Controls of Large Glacial Lakes in the Nepal Himalaya, Remote Sensing, 10, 798, 2018.

Harrison, S., Kargel, J. S., Huggel, C., Reynolds, J., Dan, H. S., Betts, R. A., Emmer, A., Glasser, N., Haritashya, U. K., and Klimeš, J.: Climate change and the global pattern of moraine-dammed glacial lake outburst floods, Cryosphere, 12, 1-28, 2018.

Immerzeel, W. W., and Bierkens, M. F. P.: Seasonal prediction of monsoon rainfall in three Asian river basins: the importance of snow cover on the Tibetan Plateau, International Journal of Climatology, 30, 1835–1842, 2010.

Kääb, A., Treichler, D., Nuth, C., and Berthier, E.: Brief Communication: Contending estimates of 2003-2008 glacier mass balance over the Pamir-Karakoram-Himalaya, Cryosphere, 9, 557-564, 2015.

King, O., Bhattacharya, A., Bhambri, R., and Bolch, T.: Glacial lakes exacerbate Himalayan glacier mass loss, Scientific Reports, 9, 2019.

Krumwiede, B. S., Kamp, U., Leonard, G. J., Kargel, J. S., and Walther, M.: Recent Glacier Changes in the Mongolian Altai Mountains: Case Studies from Munkh Khairkhan and Tavan Bogd, Global Land Ice Measurements from Space 2014, Springer, Berlin Heidelberg, 2014.

Kumar, S. P.: Estimates of the Regression Coefficient Based on Kendall"s Tau, Publications of the American Statistical Association, 63, 1379-1389, 1968.

Li, D., Shangguan, D., and Naveed, A. M.: Glacial Lake Inventory Derived from Landsat 8 OLI in 2016–2018 in China–Pakistan Economic Corridor, International Journal of Geo-Information, 9, 294, 2020.

Li, J., and Sheng, Y.: An automated scheme for glacial lake dynamics mapping using Landsat imagery and digital elevation models: A case study in the Himalayas, International Journal of Remote Sensing, 33, 5194-5213, 2012.

Liu, J. J., Cheng, Z.-L., and Su, P.-C.: The relationship between air temperature fluctuation and Glacial Lake Outburst Floods in Tibet, China, Quaternary International, 321, 78-87, 2014.

Luo, W., Zhang, G., Chen, W., and Xu, F.: Response of glacial lakes to glacier and climate changes in the western Nyainqentanglha range, Science of The Total Environment, 735, 139607, https://doi.org/10.1016/j.scitotenv.2020.139607, 2020.

Miles, E. S., Steiner, J., Willis, I., Buri, P., Immerzeel, W. W., Chesnokova, A., and Pellicciotti, F.: Pond Dynamics and Supraglacial-Englacial Connectivity on Debris-Covered Lirung Glacier, Nepal, Frontiers in Earth Science, 5, 10.3389/feart.2017.00069, 2017a.

Miles, E. S., Willis, I. C., Arnold, N. S., Steiner, J., and Pellicciotti, F.: Spatial, seasonal and interannual variability of supraglacial ponds in the Langtang Valley of Nepal, 1999–2013, Journal of Glaciology, 63, 88-105, 10.1017/jog.2016.120, 2017b.

Mueller, N., Lewis, A., Roberts, D., Ring, S., Melrose, R., Sixsmith, J., Lymburner, L., McIntyre, A., Tan, P., Curnowa, S., and Ip, A.: Water observations from space: Mapping surface water from 25years of Landsat imagery across Australia, Remote Sensing of Environment, 174, 341-352, 2016.
Neckel, N., Kropáček, J., Bolch, T., and Hochschild, V.: Glacier mass changes on the Tibetan Plateau 2003-2009 derived from ICESat laser altimetry measurements, Environmental Research Letters, 9, 468-475, 2014.
Nie, Y., Sheng, Y., Liu, Q., Liu, L., Liu, S., Zhang, Y., and Song, C.: A regional-scale assessment of Himalayan glacial lake changes using satellite observations from 1990 to 2015, Remote Sensing of Environment, 189, 1-13, 2017.
Pekel, J.-F., Cottam, A., Gorelick, N., and Belward, A. S.: High-resolution mapping of global surface water and its long-term changes, Nature, 540, 418-422, 10.1038/nature20584, 2016a.
Pekel, J. F., Cottam, A., Gorelick, N., and Belward, A. S.: High-resolution mapping of global surface water and its long-term changes, Nature, 540, 418-422, 2016b.
Qiao, L., Wanqin, G., Yong, N., Shiyin, L., and Junli, X.: Recent glacier and glacial lake changes and their interactions in the Bugyai Kangri, Southeast Tibet, Annals of Glaciology, 57, 61-69, 2016.
Quincey, D. J., Richardson, S. D., Luckman, A., Lucas, R. M., Reynolds, J. M., Hambrey, M. J., and Glasser, N. F.: Early recognition of glacial lake hazards in the Himalaya using remote sensing datasets, Global & Planetary Change, 56, 137-152, 2007.
RGI-Consortium: Randolph Glacier Inventory - A Dataset of Global Glacier Outlines: Version 6.0: Technical Report, Global Land Ice Measurements from Space, Digital Media, Colorado, USA, Digital Media, 2017.
Rounce, D., Watson, C. S., and Mckinney, D.: Identification of Hazard and Risk for Glacial Lakes in the Nepal Himalaya Using Satellite Imagery from 2000–2015, Remote Sensing, 9, 654, 2017.
Salerno, F., Thakuri, S., D'Agata, C., Smiraglia, C., Manfredi, E. C., Viviano, G., and Tartari, G.: Glacial lake distribution in the Mount Everest region: Uncertainty of measurement and conditions of formation, Global & Planetary Change, 92-93, 30-39, 2012.
Scherler, D., Bookhagen, B., and Strecker, M. R.: Spatially variable response of Himalayan glaciers to climate change affected by debris cover, Nature Geoence, 4, 156-159, 2011.
Scherler, D., Wulf, H., and Gorelick, N.: Global Assessment of Supraglacial Debris Cover Extents, Geophysical Research Letters, 45, 11798-11805, 2018.
Schiemann, R., Lüthi, D., and Schär, C.: Seasonality and interannual variability of the westerly jet in the Tibetan Plateau region, Journal of Climate, 22, 2940-2957, 2009.
Shaun D, R., and John M, R.: An overview of glacial hazards in the Himalayas, Quaternary International, 65, 31-47, 2000.
Shugar, D. H., Burr, A., Haritashya, U. K., Kargel, J. S., Watson, C. S., Kennedy, M. C., Bevington, A. R., Betts, R. A., Harrison, S., and Strattman, K.: Rapid worldwide growth of glacial lakes since 1990, Nature Climate Change, 10.1038/s41558-020-0855-4, 2020.
Song, C., Sheng, Y., Ke, L., Nie, Y., and Wang, J.: Glacial lake evolution in the southeastern Tibetan Plateau and the cause of rapid expansion of proglacial lakes linked to glacial-hydrogeomorphic processes, Journal of Hydrology, 540, 504-514, 2016.
Song, C., Sheng, Y., Wang, J., Ke, L., Madson, A., and Nie, Y.: Heterogeneous glacial lake changes and links of lake expansions to the rapid thinning of adjacent glacier termini in the Himalayas, Geomorphology, 280, 30-38, 2017a.
Song, X. P., Potapov, P. V., Krylov, A., King, L. A., Bella, C. M. D., Hudson, A., Khan, A., Adusei, B., Stehman, S. V., and Hansen, M. C.: National-scale soybean mapping and area estimation in the United States using medium resolution satellite imagery and field survey, Remote Sensing of Environment, 190, 383-395, 2017b.
Song, X. P., C, H. M., V, S. S., V, P. P., Alexandra, T., F, V. E., and R, T. J.: Global land change from 1982 to 2016, Nature, 560, 639-643, 2018.
Stehman, and SV: Impact of sample size allocation when using stratified random sampling to estimate accuracy and area of land-cover change, Remote Sens Lett, 2012.
Sudan, B. M., Pradeep, K. M., Wu, L., Gao, X., Finu, S., Rajendra, B. S., Narendra, R. K., Samjwal, R. B., Sharad, J., Sonika, S., and Prasant, B.: The status of glacial lakes in the Hindu Kush Himalaya-ICIMOD Research Report 2018/1, ICIMOD Research Report 2018/1, 2018.

Thakuri, S., Salerno, F., Bolch, T., Guyennon, N., and Tartari, G.: Factors controlling the accelerated expansion of Imja Lake, Mount Everest region, Nepal, Annals of Glaciology, 57, 245-257, 2016.

Thompson, S. S., Benn, D. I., Dennis, K., and Luckman, A.: A rapidly growing moraine-dammed glacial lake on Ngozumpa Glacier, Nepal, Geomorphology 145-146, 1-11, 2012.

Truffer, M., and Motyka, R. J.: Where glaciers meet water: Subaqueous melt and its relevance to glaciers in various settings, Reviews of Geophysics, 54, 220-239, 2016.

Ukita, J., Narama, C., Tadono, T., Yamanokuchi, T., Tomiyama, N., Kawamoto, S., Abe, C., Uda, T., Yabuki, H., and Fujita, K.: Glacial lake inventory of Bhutan using ALOS data: methods and preliminary results, Annals of Glaciology, 52, 65-71, 2011.

Wang, N., Chen, F., Yu, B., and Qin, Y.: Segmentation of large-scale remotely sensed images on a Spark platform: A strategy for handling massive image tiles with the MapReduce model, ISPRS Journal of Photogrammetry and Remote Sensing, 162, 137-147, 2020a.

Wang, X., Ding, Y., Liu, S., Jiang, L., Wu, K., Jiang, Z., and Guo, W.: Changes of glacial lakes and implications in Tian Shan, central Asia, based on remote sensing data from 1990 to 2010, Environmental Research Letters, 8, 575-591, 2013a.

Wang, X., Ding, Y. J., Liu, S. Y., Jiang, L. H., Wu, K. P., Jiang, Z. L., and Guo, W. Q.: Changes of glacial lakes and implications in Tian Shan, central Asia, based on remote sensing data from 1990 to 2010, Environmental Research Letters, 8, 575-591, 2013b.

Wang, X., Guo, X., Yang, C., Liu, Q., Wei, J., Zhang, Y., Liu, S., Zhang, Y., Jiang, Z., and Tang, Z.: Glacial lake inventory of High Mountain Asia (1990-2018) derived from Landsat images, Earth System Science Data, 1-23, doi: https://doi.org/10.5194/essd-2019-212, 2020b.

Yao, T., Thompson, L., Yang, W., Yu, W., Yang, G., Guo, X., Yang, X., Duan, K., Zhao, H., and Xu, B.: Different glacier status with atmospheric circulations in Tibetan Plateau and surroundings, Nature Climate Change, 2, 663-667, 2012.

Zhang, G., Yao, T., Xie, H., Wang, W., and Yang, W.: An inventory of glacial lakes in the Third Pole region and their changes in response to global warming, Global & Planetary Change, 131, 148-157, 2015.

Zhang, M., Chen, F., Tian, B., Liang, D., and Yang, A.: High-frequency glacial lake mapping using time series of sentinel-1A/1B SAR imagery: An assessment for the southeastern tibetan plateau, International Journal of Environmental Research and Public Health, 17, 1072, 2020.

Zhao, H., Chen, F., and Zhang, M.: A Systematic Extraction Approach for Mapping Glacial Lakes in High Mountain Regions of Asia, IEEE Journal of Selected Topics in Applied Earth Observations and Remote Sensing, 11, 2788-2799, 10.1109/JSTARS.2018.2846551, 2018.

Zhu, Z., and Woodcock, C. E.: Object-based cloud and cloud shadow detection in Landsat imagery, Remote Sensing of Environment, 118, 83-94, 2012.

Chen, F., Zhang, M., Guo, H., Allen, S., Kargel, J., Haritashya, U., Watson, S.: Annual 30-meter Dataset for Glacial Lakes in High Mountain Asia from 2008 to 2017 (Hi-MAG) [Dataset], Zenodo, https://doi.org/10.5281/zenodo.4059181.